Polymeric Dynamic Crosslinker for Upcycling of Fragile Low Molecular Weight Polypropylene

Mikaela Sadri^{1, #}, Shalin Patil^{2, #}, Jonathan Perkins¹, Zoe Gunter¹, Shiwang Cheng^{2,*}, Zhe Qiang^{1,*}

Correspondence to: S. C. (Email: chengsh9@msu.edu); Z. Q. (Email: zhe.qiang@usm.edu)

Abstract

While tremendous progress has been made in the dynamic crosslinking of polypropylene (PP) for plastics upcycling, their efficacy in addressing low molecular weight (MW) PP waste remains untapped. In this work, we demonstrate a simple and scalable method to convert brittle low MW PP to vitrimer materials with enhanced thermal and mechanical properties, enabling their use in circular upcycling. Different from most previous work employing small molecule crosslinkers, we prepare PP vitrimers (PP_v) using polymeric crosslinkers, containing polyethylene glycol segments (PEG), which lead to altered crystalline structures and network formation. Importantly, by increasing the MW of crosslinkers from 200 Da to 1000 Da, the PP_v exhibit more than 50 times increase in their fracture energy with strong ductility, which can be attributed to combined effects of strengthened amorphous regions of semi-crystalline PP domains and the phase separation between soft PEG segments and PP matrix. Moreover, when blending the PP_v with high MW PP (PP_h), the PP_h/PP_v blends show comparable elastic modulus, yield strength, and stretchability to the PP_h, in sharp contrast to the widely-known embrittlement of low MW PP/PP_h blends. These results demonstrate the use of polymeric dynamic crosslinkers as an important strategy for upcycling low MW PP waste to value-added products.

Keywords: polyolefin, vitrimers, crystallinity, circular economy, structure-property relationship

1. Introduction

Polypropylene (PP) is ubiquitous and widely used in numerous applications, such as food packaging, ^{1–3} automotive parts, ⁴ and medical supplies. ^{5,6} With a global PP production exceeding over 75 million metric tons in 2021, less than 10 % was recycled and the rest was landfilled, incinerated, or improperly discarded. ⁷ Since PP is very difficult to decompose in the natural environment, once mobilized the waste can form microplastics and leach into the ocean, soil, and aquatic sediments, imposing significant environmental and health threats on human society and marine ecosystems. ^{8–10}

Significant efforts have been focused on PP waste recycling and upcycling, aiming to convert them to products with equal or higher value. 11-13 Mechanical recycling is energy efficient and allows the reuse of PP for new products, but it often leads to reduced viscosity and molecular weight (MW) due to thermally and/or mechanically induced chain scissions. 14,15 As a result, PP shows continually degraded properties upon recycling, which can become too brittle to meet the

¹School of Polymer Science and Engineering, The University of Southern Mississippi, Hattiesburg, MS, US, 39406

²Department of Chemical Engineering and Materials Science, Michigan State University, East Lansing, MI, US, 48864

requirement for practical applications. Chemical upcycling provides alternative approaches to convert PP waste to products with altered chemical identity and properties. Among many chemical upcycling methods, direct functionalization represents a promising solution, potentially more energy-efficient than pyrolysis methods, through incorporating functional groups on PP for achieving value enhancement.¹⁶ Particularly, converting commodity thermoplastics to vitrimers through introducing dynamic crosslinkers using reversible chemical bonds has received significant attention in recent years.¹⁷ Specifically, vitrimers are an emerging class of crosslinked materials with unique reprocessability, enabled by associative dynamic bond-exchange mechanism, which can retain the same crosslinking density at elevated reprocessing temperatures. Over the past few years, a number of vitrimer chemistries have been demonstrated with polyolefins, such as transesterification,^{18, 19} disulfide crosslinking,^{20, 21} imine exchange,^{22, 23} thio-anhydride,²⁴ silyl ether exchange,^{25, 26} and dioxaborolane metathesis;^{27–29} most rely on reactive extrusion to simultaneously process and functionalize plastics. A recent review article by Ahmadi et al., systematically discussed recent progress in polyolefin-based vitrimers.³⁰

Despite the success in developing polyolefin-based vitrimers, understandings about the influence of network formation on the polymer crystallization behaviors and crystal morphology remain relatively limited.^{31, 32} Soman et al., found that dynamic crosslinking of olefinic oligomers with small molecule crosslinkers can largely influence their crystallization behaviors.³³ However, opportunity of using polymeric crosslinkers for commodity polyolefin-to-vitrimer conversion is still underexplored. Particularly, polymeric crosslinkers may result in microscopic phase separation in vitrimers due to their high immiscibility with matrix, potentially providing additional opportunities to alter material properties through controlling their phase separation behaviors. In a recent work by Ji et al., di-functional, low MW polyesters were employed for dynamically crosslinking high MW polyethylene (PE),³⁴ however, improved performance was not obtained compared to starting materials.

Inspired by and building on previous research progress, we found three critical opportunities for enabling improved use and transformative impact of PP chemical upcycling methods. First, feedstock selection (e.g., targeted waste type) is a key component in technology design and implementation. Most studies associated with PP upcycling focused on commodity materials, which have high MW, good processability, and excellent mechanical performance. However, their use for addressing poor-value waste, such as their brittle low MW counterparts remains unclear, although their chemical upcycling represents a critical and urgent need. Second, many reports of converting high MW PP to vitrimers show the derived products having comparable properties to their virgin counterparts. It is desired to extend or establish technologies that can improve the properties of low MW waste, which would be more impactful to the polymer industry.³⁵ Third, the recycling system design should accommodate other environmental considerations for materials synthesis and processing.³⁶ For example, previous works of synthesizing polyolefin vitrimers were often based on transesterification chemistry employing bisphenol A (BPA)-based chemicals as the crosslinkers. If BPA concentration is high, it could be potentially harmful to human health, including the hormone system, brain, and reproductive organs.³⁷ Therefore, the need for new crosslinker chemistry (i.e., BPA-free) for PP vitrimer synthesis is apparent.³⁸

This work collectively addresses these important challenges and opportunities by demonstrating a robust strategy that converts fragile PP to vitrimers through reactive extrusion, allowing their further and enhanced use in plastic upcycling. In particular, the purposeful selection of low MW PP as the starting material represents plastic waste with very limited value and use.

Distinct from most previous efforts of polyolefin vitrimer synthesis using small molecule crosslinkers, we employ polymeric dynamic crosslinkers and focus on understanding the impacts of their MW and loading content on the gel fraction, crystallization, and morphology of resulting vitrimers. It is observed that polymeric dynamic crosslinkers can efficiently alter the amorphous domains (structures and properties) of PP vitrimers, enabling significantly enhanced mechanical properties, including toughness, yield strength, and ductility. Gratifyingly, the upcycled PP vitrimers, when serving as a minority component blended with high MW PP (PPh), do not lead to embrittlement of PPh as the virgin low MW PP does, providing a working protocol to fulfill the recent government mandate of containing 15% post-consumer resin (PCR) in new product manufacturing. These results demonstrate that polymeric dynamic crosslinkers can be fundamentally different from small molecule crosslinkers for controlling the macroscopic properties of vitrimers, providing a new avenue for utilizing dynamic network chemistry to upcycle PP waste.

2. Experimental Section

2.1 Materials

Low MW polypropylene-*graft*-maleic anhydride (PPg, number-average molecular weight, M_n : 3,900 Da, maleic anhydride (MA) content: ~6 wt% determined by titration), zinc acetylacetonate hydrate (Zn(acac)₂), and phenolphthalein were purchased from Sigma-Aldrich. Poly(ethylene glycol) diglycidyl ether (PEGDGE) with two molecular weights (MW), 200 Da and 1,000 Da, were purchased from Polysciences, Inc., and referred to as PEG200 and PEG1000. Xylene (99 %) was obtained from Thermo Scientific. Ethanol (190 proof) was obtained from Decon Laboratories, Inc., and potassium hydroxide (KOH, 85 %) was purchased from Alfa Aesar. PP (extrusion-grade, high MW commodity plastic, noted as PPh, which has a viscosity-average molecular weight of approximately 1.6×10^5 g/mol) was obtained from Muehlstein. All chemicals were used as received unless otherwise noted.

2.2 Sample preparations

All formulations were mixed and compounded by an Xplore MC5 microcompounder at 147-160 °C at a screw speed of 80 rpm. In a typical process, PP_g (3 g) was first introduced into the microcompounder, followed by adding a blend of di-epoxide terminated crosslinkers (PEG200 or PEG1000) and catalyst ($Zn(acac)_2$, 1 wt% of the PP amount) with controlled molar ratio, including 0.8, 1.2, and 1.6. The residence time for the reactive extrusion was determined through the force output that is related to the viscosity of the compounding materials. Total processing time was varied from 10 - 30 min to achieve the force plateau as the crosslinker content changed. Details of the material composition and processing condition for each vitrimer are provided in **Table S1**. We refer to the vitrimer samples as PP_v -x-y, in which x represents the MW of PEGDGE, and y is the molar ratio of epoxide (from PEGDGE) to MA groups (from PP_g).

2.3 Materials characterization

The MA content of the PP_g was determined *via* titration. PP_g (0.5 g) was refluxed in xylenes (150 mL) at 130 °C until PP_g was completely dissolved. Approximately 0.25 mL of water was then

added dropwise to the PP_g/xy lene solution before titration with 0.05 M KOH solution, using phenolphthalein as the indicator. The MA content (G), in weight percent, was calculated *via* the following equations:

$$A. N. = \frac{(V)(M)(M_{n,KOH})}{m_{poly}},\tag{1}$$

$$G = \frac{(\frac{A.N.}{1000})(M_{n,MA})}{(2M_{n,KOH})} \times 100\%, \tag{2}$$

where A.N. is the acid number, otherwise known as the mass of KOH (unit: mg) required to neutralize one gram of PP_g. V is the volume of KOH titrant added, M is the molarity of titrant, M_n is the molar mass of the specified component, and m_{poly} is the mass of polymer used in the analyte. $M_{n,KOH}$ is multiplied by two in Eq.2 to account for the dual acidic groups of MA.

A solvent extraction method was used to determine the gel fraction of the vitrimer networks. Specifically, the vitrimers were submerged in hot xylene at 120 °C for 24 h. Subsequently, the insoluble fraction was removed from the vitrimer/xylene mixture and dried under vacuum overnight. The gel fraction was then calculated via the following equation:

$$gel\ fraction = \left(\frac{w_f}{w_i}\right) \times 100\%,$$
 (3)

where w_i and w_f are the mass before and after solvent extraction, respectively.

Fourier transfer-infrared (FT-IR) spectroscopy was performed on solid vitrimer samples using a PerkinElmer FT-IR spectrometer with the universal attenuated total reflectance (ATR) sampling accessory attached. Scans were taken from 4000 to 600 cm⁻¹ at a resolution of 4 cm⁻¹ and an average of 32 scans. The thermal stability of vitrimers was determined *via* thermogravimetric analysis (TGA) using a TGA Q50 (TA instrument). In platinum pans, 10 – 15 mg vitrimer samples were heated under nitrogen at 10 °C/min up to 600 °C. The temperature at which 5 % mass loss occurred (T_{d5}) was recorded. The melting and crystallization temperatures (T_m and T_c) of samples were characterized using differential scanning calorimetry (DSC), which is a TA Instruments Discovery DSC250. Tzero pans and lids (from TA instruments) were used, and a heat-cool-heat cycle was employed with a temperature profile ranging from -50 °C to 200 °C at a ramp rate of 10 °C/min. T_c and T_m were determined by the temperature at the peak heat flow from the second and third step, respectively, and the degree of crystallinity (*X_c*) was calculated using the following equation:

$$X_c = \left(\frac{\Delta H_f}{\Delta H_f^0}\right) \times 100\%,\tag{4}$$

where ΔH_f is the enthalpy of fusion and $\Delta H_f^0 = 209 J/g$ is the standard enthalpy of fusion of PP_g. Both TGA and DSC data acquisitions and analysis were carried out using Trios software.

Rheological and tensile samples (ASTM 638 type IV bars for tensile testing) were prepared using a Carver 4386 press. Linear rheology was performed on an Anton Paar MCR302 rheometer with a CTD 600 oven. The accuracy of the temperature control was \pm 0.1 K. Small amplitude oscillatory shear (SAOS) tests were performed on a pair of 8 mm parallel plates with a gap of 1 mm and a temperature range from 160 °C to 80 °C at a temperature interval of 10 °C. The samples were loaded and tested at 160 °C (above the melting point of PP) before subsequent tests at lower temperatures. To ensure thermal equilibrium, the samples were annealed at each testing temperature for at least 20 minutes before the test. The strain amplitude was chosen to be 5% at 160 °C and gradually reduces to 0.05 % for the temperature of 80 °C. We would like to note that the SAOS measurement of polymers and filled polymers can be made to modulus of \sim 10 Pa that is at least one order of magnitude higher than the shear modulus of semi-crystalline polymers in

this study.³⁹ In our systems, all PP_v samples had high fractions of amorphous region ($\sim 80 \text{ v}\%$) that facilitate the SAOS measurements. To examine the influence of wall-slip in the SAOS measurements for the PPv samples, we varied the testing gap from 0.80 mm to 0.95 mm and observed negligible changes in shear modulus (**Figure S1**). These results supported the absence of wall-slip in the tests, even at the lowest temperatures of 80 °C. The testing frequency was set as 10^2 rad/s to 10^{-1} rad/s. The step-strain relaxation of vitrimers took place at 165 °C in the same 8 mm parallel plate geometry at a strain unit of 5 % and a strain rate of 0.01 s^{-1} .

For the tensile testing, PP_g and their derived vitrimers were melt pressed at 175 °C for a total of 15 min (10 min heating with no pressure, 3 min under 10 MPa, and 2 min under 25 MPa) before cooling on an aluminum bench with a steel heatsink on top, holding the mold together. Uniaxial extension tests of PP_v were performed on an RSA-III solid analyzer at a constant crosshead speed of 0.01 mm/s. Rectangular-shaped sample strips were employed in the measurements with an initial sample length of 10 mm and sample thickness of 0.1 – 0.15 mm. The strips were pressed at 160 °C in a Carver Press and quenched to room temperature through air cooling. For blend samples containing PP_h as the majority component, tensile tests were performed using an MTS Insight frame with a 500 N load cell at 5 mm/min at room temperature, based on ASTM 638 with a type IV tensile bar. Data analysis was performed on Igor Pro 9, where the ultimate tensile strength (UTS) was determined by the maximum tensile stress achieved before sample failure, the elastic modulus was calculated as the slope of the linear region of the curve prior to yield, and the toughness was determined by integrating the stress-strain curves for each sample.

X-ray scattering measurements were performed at the beamline 12-ID-B at Advanced Photon Source of Argonne National Laboratory with an X-ray energy of 13.3 keV (λ_{x-ray} = 0.9347 Å). The scattered X-ray signals were collected using a two-dimensional Pilatus 2M detector. The sample-to-detector distance was set to be at 2.0 m and the detecting range of the scattering wave vector, q, covers from 0.003 to 0.9 Å⁻¹. For all measurements, the sample thickness (solid thin film at 25 °C) was in the range of 0.1-0.15 mm and the exposure time was 1 s. The absolute intensity of X-ray scattering was calibrated using glassy carbon, and the values of detector pixels were calibrated using silver behenate. The background signal was collected using an empty sample hole at the same testing conditions. The presented intensities in this work were all after subtraction of the background scattering. Polarized optical microscopy (POM) (Nikon Eclipse ME600) with a temperature controller (Instec mK1000, HCS302) was employed to characterize the crystalline morphology of the PP_g and the PP_v at temperatures from 160 °C to 30 °C. Isothermal crystallization of PP_h, PP_h/PP_g blends, and PP_h/PP_v blends were performed under POM at 125 °C using the same optical setup. The temperature controller has an accuracy of \pm 0.1 °C. All the polarized images were taken by a Q-Imaging RoHS Camera (2048 pixel ×1536 pixel) in a transmission mode at a 90° angle configuration between the linear polarizer and the linear analyzer.

3. Results and Discussions

3.1 Synthesis of PP vitrimers using PEGDGE as dynamic crosslinkers

Figure 1 presents the synthesis scheme of converting PP_g into vitrimers (i.e. PP_v) through epoxy-anhydride reaction. Specifically, di-epoxide functionalized PEG (i.e., PEGDGE) was employed as the crosslinking agent, which reacted with the MA group under the presence of (Zn(acac)₂) (**Figure 1a**) at temperatures higher than 150 °C. The crosslinking reaction, conducted

through reactive extrusion, can be confirmed by the force output on the screws reaching a plateau value (**Figure S2**). The ester bonds (served as crosslinkers) are thermally reversible through the associative bond exchange mechanism with the presence of a catalyst (**Figure 1b and Figure S3**). ^{40,41} Different molar ratios of epoxide (from PEGDGE) to maleic anhydride (MA), such as 0.8, 1.2, and 1.6, were prepared for understanding the influence of polymeric crosslinker loading on resulting material properties. In this work, low MW PP_g is brittle and can hardly form a film due to a lack of chain entanglements, which was purposely selected as the starting material, known as the (undesired) product generated from the mechanical recycling of commodity PP. ^{42, 43}

Figure 1. (a) The reaction scheme of the crosslinking reaction of PP_g and PEGDGE, where Zn(acac)₂ is the catalyst to enable (b) thermally reversible transesterification reactions of vitrimers.

FT-IR was performed to confirm the epoxy-anhydride reaction. As shown in **Figure 2**, neat PP_g has vibrational bands of alkane (C-H) stretching and bending at 2840-2950 cm⁻¹ and 1375-1460 cm⁻¹, respectively, along with bands at 1730-1780 cm⁻¹ from the C=O bonds in the anhydrides. The introduction of PEG200 or PEG1000 to PP_g results in a band at 1100 cm⁻¹, corresponding to the C-O bonds. Upon crosslinking with PEGDGE, the intensity of the band at 1730 cm⁻¹ began to increase due to the formation of ester bonds. The appearance of C-O and O-H bands, in addition to the shifting of the carbonyl bands from the anhydride to an ester, confirms the successful epoxy-anhydride reaction between PP_g and PEGDGE. Consequently, the band intensities at 1780 cm⁻¹ and 1850 cm⁻¹, associated with the symmetric and asymmetric C=O stretching of the anhydrides respectively, were both decreased, suggesting the esters were formed from the anhydride groups. Additionally, after crosslinking reaction, a slight increase in the absorbance at 3500 cm⁻¹ (corresponding to alcohol groups) for the PEG200 crosslinked samples was observed (also highlighted in **Figure S4**), which was more pronounced when the PEG1000 was incorporated; these observations indicate a higher -OH content in PP_v-1000 samples.

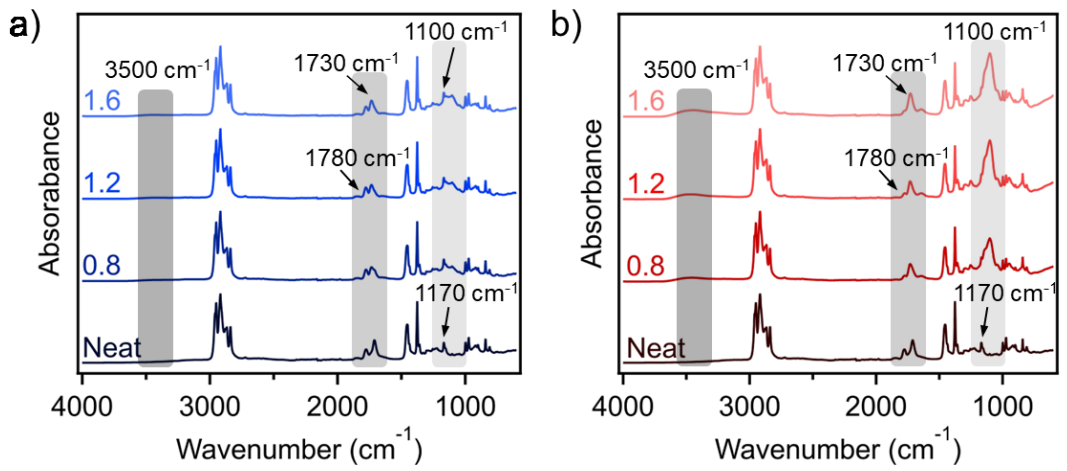


Figure 2. FT-IR spectra of PP_g (neat) and PP_v with varying molar ratios of epoxides to MA using (a) PEG200, and (b) PEG1000 as crosslinkers. Different IR bands corresponding to epoxyanhydride reactions are highlighted in grey.

To further confirm the network formation, xylene extraction was performed to quantify the gel content. As shown in Figure 3, the control sample PPg was completely dissolved after 24 h soaking in hot xylene. In contrast, insoluble parts can be obtained from PP_v. The insoluble fraction increases with a higher amount of PEGDGE crosslinkers. These observations are consistent with the FT-IR results, indicating an increased degree of crosslinking. Additionally, it is found that a higher gel content can be obtained with PEG1000 than with PEG200 at the same [PEG]/[MA] molar ratio. For example, PP_v-200-0.8 has a gel fraction of 16 wt%, which is much lower than the 26 wt% of PP_v-1000-0.8. Increasing [PEG]/[MA] ratio to 1.2 and 1.6 results in a gel fraction of 24 wt% and 35 wt% of PP_v-200 vitrimers, and 34 wt% and 40 wt% of PP_v-1000 vitrimers, respectively. The gel fractions obtained in this system, from 16 wt% to 40 wt%, were in a similar range compared to previous literature results. 18 The higher gel content for a high MW PEG dynamics crosslinker is interesting and suggests a higher integration of PEG1000 than PEG200 to the PP matrix. One possible reason of the higher reactivity of higher MW PEG crosslinkers might be associated with their slower kinetics for phase separation of PP/PEG. As a result, the higher MW PEG can have a longer contact time with PP to promote the chemical reaction under shear.⁴⁴, ⁴⁵ These observations are also consistent with a higher force output (after reactive extrusion reaction) of PP_v-1000 than PP_v-200 samples (Figure S5).

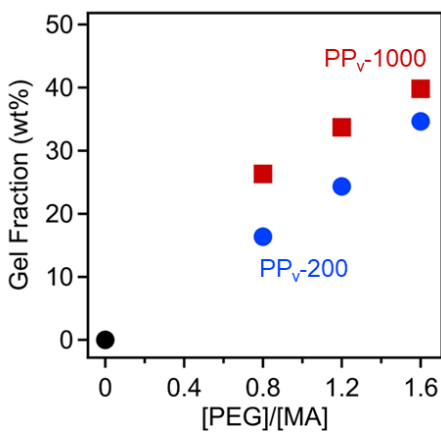


Figure 3. Gel fraction was determined through a solvent extraction method using xylene at 120 °C for 24 h, where PP_v -200 samples are shown in blue circles, PP_v -1000 samples are shown in red squares, and neat PP_g is a black circle for reference.

3.2. Thermal properties of PP_v

TGA (**Figure S6**) was first performed to understand the thermal stability of PP-based vitrimers. It was found that all PP_v materials had a higher T_{d5} than the neat PP_g (**Figure 4**). Specifically, T_{d5} increased from 245 °C for PP_g to 259 °C and 294 °C for PP_v-200-0.8 and PP_v-1000-0.8, respectively. The T_{d5} also generally increased with increasing crosslinker content from 0.8 to 1.6 for both PEG200 and PEG1000, in which T_{d5} of PP_v-200-1.6 increased to 278 °C and that of PP_v-1000-1.6 increased to 299 °C. It should also be noted that the T_{d5} of PP_v-1000 series was higher than the PP_v-200 samples at the same [PEG]/[MA] ratio, which is a result of the increased thermal stability of neat PEG1000 compared with PEG200 (**Figure S6**). Among all PP vitrimer samples, T_{d5} of PP_v-1000-1.6 is the highest, comparable to commodity, high MW PP, showing that on-set degradation temperature of PP can be significantly improved (an increment of ~50 °C) by creating vitrimer networks, likely a result of the significant increase in MW as it forms a network.^{51,52}

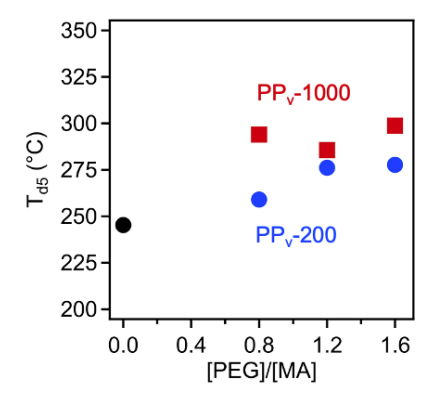


Figure 4. T_{d5} of PP_g and PP_v as a function of PEGDGE molecular weight and loading content. PP_g is a black circle for reference.

Additionally, differential scanning calorimetry (DSC) was performed to understand the crystallization behaviors of PP_v. Figures 5(a) and (b) show the crystallization of PP_v in the cooling process after thermal annealing at high temperatures. A crystallization peak in the temperature window of 100 °C - 125 °C is observed for all PP_v. Specifically, T_c (determined from the peak position) for PPg was 107 °C and increased to 110 °C and 111 °C for PPv-200-0.8 and PPv-1000-0.8, respectively, and further increased to 114 °C and 115 °C for PP_v-200-1.6 and PP_v-1000-1.6 samples (Figure S7). The similar T_c for both PP_v-200 and PP_v-1000 samples suggest that the MW of the crosslinker has a very limited influence on T_c while the PEGDGE loading level has a larger impact. No crystallization peak of PEG was observed in these samples, indicating the formation of vitrimer suppresses the PEG crystallization. Note that the neat PEG1000 has a sharp recrystallization peak at 15 °C and the PEG200 is not able to crystallize (Figure S8). Interestingly, upon second heating, a cold re-crystallization followed by melting of PEG1000 was observed for PP_v-1000-1.2 and PP_v-1000-1.6, while there is no obvious cold recrystallization taking place for PP_v-1000-0.8 or any of the PP_v-200 samples (Figures 5(c) and (d)). The lack of re-crystallization of PEG in PP_v-200 is anticipated since the neat PEG200 is amorphous. However, the emergence of cold re-crystallization of the PEG component (observed in samples PP_v-1000-1.2 and PP_v-1000-1.6) suggests the presence of phase separation between PEG segments and PP matrix, which occurred due to their limited miscibility. 46, 47

The use of PEG crosslinkers slightly alters the degree of crystallinity ($X_{c,PP}$) of the PP phase. As demonstrated in **Figure S9**, the neat PP_g has a crystallinity degree of ~39 %, which was slightly reduced to ~36 % for PP_v-200-1.6 and ~32 % for PP_v-1000-1.6 vitrimers. The limited reduction in $X_{c,PP}$ for these materials further suggests phase separation between the PP and PEG components. Additionally, the slightly larger influence of the PEG1000 than the PEG200 on the crystallinity of PP is likely a result of a higher fraction of PEG1000 than PEG200 in the PP matrix at the same molar ratio of [PEG]/[MA]. We note similar observations of a reduction in crystallinity of polyolefin vitrimers have been observed in other systems. For instance, both Khonakdar et al. ⁴⁸ and Krumova et al. ⁴⁹ found that when increasing the organic peroxide, the polymer network crystallinity would decrease. By increasing the crosslinker loading, slightly increased portions of PP_v chains were unable to crystallize, and this effect becomes further pronounced when employing a higher molecular weight PEGDGE as the crosslinker. These results indicate that using a telechelic polymer (i.e., PEG) to crosslink PP_g can also disrupt the crystallization behaviors of PP.

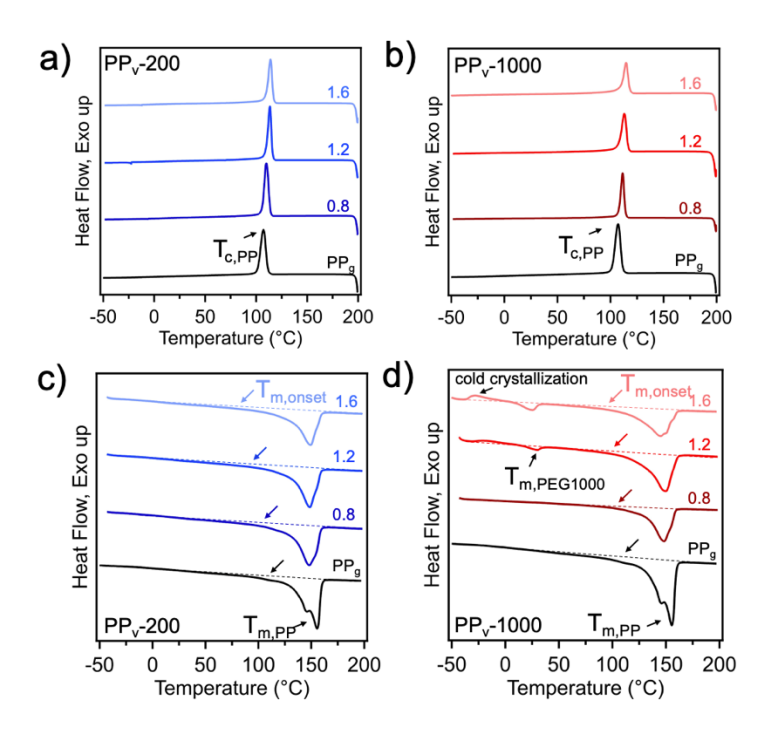


Figure 5. DSC thermograms of (a) PP_v-200 and (b) PP_v-1000 samples during cooling, as well as the 2nd heating curve of (c) PP_v-200 and (d) PP_v-1000 samples. The heating curves include representative baselines (dashed lines) across the thermograms to illustrate changing onset of melt.

3.3 Structural characterization of PP_v.

To be more quantitative, we analyzed the T_m of the vitrimers to determine their crystal morphology. As shown in **Figures 5(c) and (d)**, T_m of the PP phase in PP_v is lower than its neat counterpart, PP_g, which is related to the crystal lamellae thickness, as described through the Gibbs-Thomson equation:

$$T_m = T_m^0 \left(1 - \frac{2\sigma_e}{\Delta H_0^0 L} \right), \tag{5}$$

where T_m is the observed melting temperature (peak value, unit in K) for a crystalline lamella of thickness L, T_m^0 is the equilibrium melting temperature of PP (unit in K), ΔH_f^0 is the enthalpy of fusion for the crystalline phase, and σ_e is the surface energy of the basal surface of a lamellar crystal. Using T_m in conjunction with the following values obtained from literature, the lamellar thickness, L, was estimated for each sample ($T_m^0 = 481$ K, which equals 208 °C, $\sigma_e = 62.3 \times 10^{-7}$ J/cm², and $\Delta H_f^0 = 209$ J/g). ^{50,51} Through these calculations, we found the average L decreased from 5.5 nm for PP_g to 4.9 nm for PP_v-200-0.8 and PP_v-1000-0.8, as a result of incorporating dynamic crosslinkers and conversion of linear polymers to networks. Furthermore, T_m of the PP phase in all PP_v were all very similar, regardless of PEG MW and loading content, corresponding to a very similar L in the range between 4.8 nm and 5.0 nm (**Table S2**).

While the lamellar thickness can be obtained using the peak of the melting endotherm, $T_m - T_{m,onset}$ can also be used to evaluate PP crystal morphology, where a lower value indicates more uniform/perfect crystal formation.⁵² It can be observed that in **Figures 5(c) and (d)**, both T_m , onset decrease from 141 °C for PP_g to 131 °C for PP_v-200-0.8 and 132 °C for PP_v-1000-0.8,

respectively, while their T_m was at 155 °C, 148 °C, and 148 °C, respectively. Additionally, by increasing the crosslinker molar ratio in both PP_v -200 and PP_v -1000, a larger $T_m - T_{m,onset}$ was found, suggesting an increment in the size distribution of the lamellar thicknesses of these samples. Additionally, lamellar thickness distribution of these PP crystals can also be determined via following equation:⁵³

$$\frac{1}{M}\frac{dM}{dL} = \frac{dE}{dT}\frac{(T_m^0 - T_m)^2 \rho_c}{2\sigma_e T_m},\tag{6}$$

where M refers to the mass of the crystalline phase within the sample, dE/dT is the energy necessary to melt the dM portion of the crystalline phase, obtained from the DSC endotherm, ρ_c is the density of the crystal phase, and the other parameters are defined the same as in equation 5. Using this equation, distributions of lamellae thickness for all PP_v samples and PP_g are determined and provided in **Figure S10**, which the averaged *L* agrees well with results determined by Gibbs-Thomson equation. Furthermore, a slightly broadening of peak was observed for PP_v-1000 samples with increased content of PEGDGE crosslinkers.

To gain further insights into the crystal sizes and the phase separation between PP and PEG segments, we performed small angle X-ray scattering (SAXS) on PP_v-200 and PP_v-1000 samples, as well as PPg as the control. Lorentz corrected scattering intensity as a function of scattering wavevector q (from SAXS measurements) of these materials was plotted as shown in Figure 6, which can be used to evaluate the influence of PEGDGE crosslinkers on the long period, d, of the PP lamellar structure. A clear shift of the peak towards a lower q region is observed for PP_v-200 and PP_v-1000 vitrimers than the neat PP_g; the higher the PEGDGE content, the larger the shift was found. Moreover, PP_v-1000 exhibits a much stronger shift to the low q than the PP_v-200, while the correlation peak is also much sharper at the same [PEG]/[MA] molar ratio. The shift in characteristic peak location corresponds to a significant increase in d after converting PP from linear to network structures, increasing from ~10 nm (PP_g) to ~15 nm and ~29 nm for PP_v-200-1.6 and PP_v-1000-1.6, respectively (**Table S2**). These results, along with the lamellar thickness of PP determined by DSC (which shows a small reduction after converting PPg to PPv), indicate that PEGDGE crosslinkers strongly influence the amorphous regions and the crystallinity with increasing crosslinker MW and/or loading content. 54,55 These observations are also consistent with the shift of the crystal onset melting temperature towards lower values. Collectively, our results show that by using polymeric crosslinkers, the morphology of semi-crystalline PP can be successfully engineered, providing a pathway to control their mechanical performance. We would like to note that previous studies of polyolefin vitrimers often focused on characterizing their temperature- and strain-dependent viscoelastic responses for understanding the impact of dynamic crosslinkers; yet the correlation between their crystalline morphology and material properties remains underexplored. Since both the lamellae thickness and the degree of crystallinity are critical for the mechanical properties of semi-crystalline polymers, one would anticipate a large influence of the PEGDGE crosslinkers on the mechanical properties of resulting vitrimer materials, which we will discuss in detail in the following section.

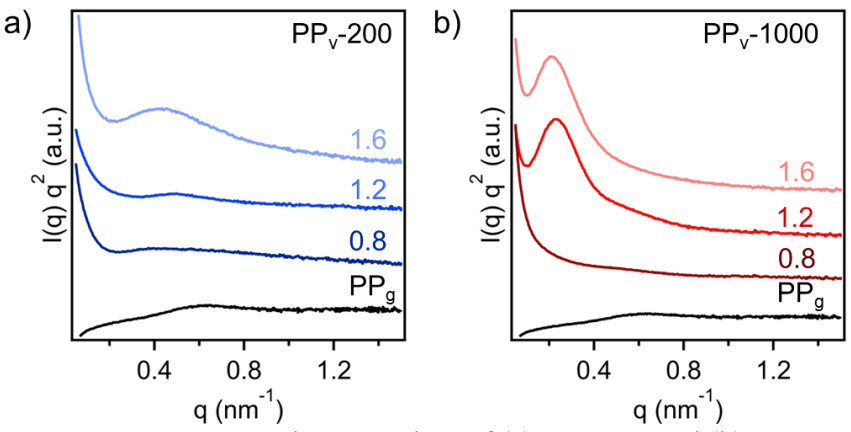


Figure 6. Lorentz corrected SAXS plots of (a) PP_v -200 and (b) PP_v -1000 samples. PP_g as a control sample is also included

Another important feature from the SAXS patterns in Figure 6 and Figure S11 is the strong upturn of the scattering intensity at the low q region ($< 0.06 \text{ nm}^{-1}$), suggesting the presence of features with sizes larger than 100 nm in all PP_v. The nature of such features in our system could arise from multiple mechanisms, such as large lamellae crystals of PP, phase separation between PP and PEG, or high structural heterogeneity of crosslinked network. Given the leveling-off of the scattering intensity at the low q region from neat PPg, it is unlikely that the low q upturn of PPv is from PP crystals. To examine another possibility of phase separation within PP_v, polarized optical microscopy (POM) was employed to study their morphologies. Figure 7 shows the optical images of neat PP_g (Figure 7 (a)), PP_v-200-1.6 (Figure 7 (b)), and PP_v-1000-1.6 (Figure 7(c)) at 100 °C. These two compositions were selected as higher PEGDGE content could provide a greater opportunity for phase separation to occur. Figure 7(a) shows the classical polycrystalline morphology of PPg that fills the whole field of view. The bright and dark parts represent different crystal orientations to the incoming polarized light. For PPv samples, both Figure 7 (b) and (c) show significant phase separations between bright and dark regions, indicating the spatially heterogeneous network structures. Moreover, while the crystalline domain of PP is observed, there are no clear resolutions of the Maltese cross, suggesting the incorporation of PEG crosslinker strongly influences the packaging of the crystal lamellae. Interestingly, cooling the sample of PP_v-1000-1.6 down to temperatures below the melting temperature of PEG, i.e. 30 °C or lower, does not promote further crystallization in the dark region (Figure 7(d)), indicating a strong suppression of PEG crystallization in PP_v. We note that DSC measurements of PP_v-1000-1.6 sample show signatures of phase separation between PP and PEG segments as cold re-crystallization of PEG of segment was occurred. Therefore, we believe that the upturn of scattering intensity at low q region is associated with phase separation between PEG minority phase and PP matrix, creating PP-rich and PEG-rich domains.

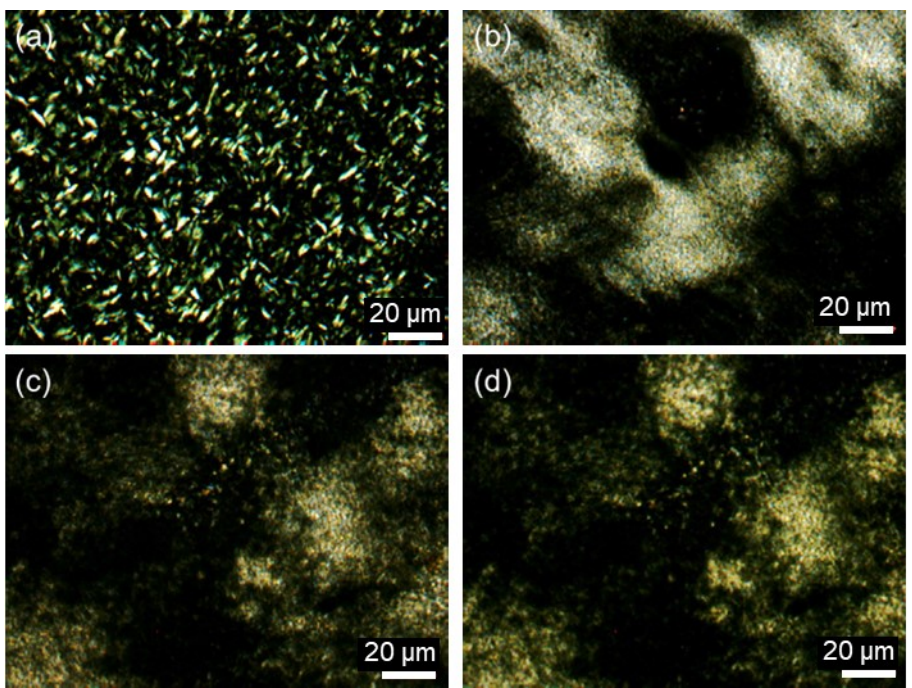


Figure 7. Polarized optical microscopy images of (a) neat PP_g at 100 °C, (b) PP_v-200-1.6 vitrimer at 100 °C, (c) PP_v-1000-1.6 vitrimer at 100 °C, and (d) PP_v-1000-1.6 vitrimer at 30 °C. The neat PP_g crystals cover the whole field of view. Strong structural heterogeneities were observed in the morphologies (the bright region and the dark region) for PP_v-200-1.6 and PP_v-1000-1.6 vitrimers. Scale bar: 20 μm

Moreover, WAXS results (**Figure S12**) indicate that for both PP_v-200 and PP_v-1000 samples, the crystallization of PP is well resolved and there is little evidence of the PEG crystallization. This is consistent with the suppressed crystallinity of PEG in all vitrimers (the highest PEG crystallinity is only at \sim 3 %, in PP_v-1000-1.6, according to DSC). Including PEGDGE crosslinkers does not yield any new crystalline phases in the PP systems. Moreover, while the characteristic peaks of PP_v have identical 20 values compared to those of neat PP_g, they were slightly narrow in PP_v, indicating an increase in the average crystal size. Notably, the significantly increased crystal size of PP_v-200-0.8 can be attributed to the addition of a low amount PEG200 (\sim 4 vol%); a small number of polymeric additives employed for promoting PP crystallization was also observed in previous studies. ⁵⁶⁻⁵⁸

3.4. Mechanical properties of PP_v.

To quantify the impact of the polymeric crosslinkers on the viscoelastic properties and the mechanical properties of the PP_v, we performed linear viscoelastic measurements and tensile deformation. **Figure 8** presents the storage modulus, G', and loss modulus, G'', from SAOS measurements of PP_v at 100 °C, 130 °C, and 160 °C, while additional data was included in **Figures S13** and **S14** to reveal more detailed temperature-responsive behaviors. At temperatures below 130 °C, a $G' \sim G'' \sim \omega^{0.06}$ is observed with $tan\delta \sim 0.1$, indicating the solid-state response of PP_v that is typically observed in semi-crystalline polymers below their T_m. At temperatures above 130 °C, a significant amount of PP lamellae melts and a sharp drop in elastic modulus was observed from

 10^8 - 10^7 Pa to 10^5 - 10^4 Pa. In principle, one should be able to extract the molecular weight between crosslinking points from the high-temperature (above the melting point) modulus plateau. However, the phase separation between PEG and PP makes it challenging to perform quantitative determinations since the soft domains can also lead to a modulus plateau. ⁵⁹ Assuming the plateau modulus at high temperatures to purely from the elasticity of the network strands, a molecular weight between crosslinking points (the lower bound) of ~11 kg/mol can be obtained by assuming mass density $\rho = 0.791$ g/cm³ and gel fraction of 40% of PP_v, ⁶⁰ implying a combination of PEG and PP in the network strands. While the crosslinking density and the molecular weight between crosslinking points should also be able to quantify through swelling-based experiments, we note that PP_v samples can precipitate out upon cooling from high temperature (120 °C) swelling in xylene, rendering it impractical to identify the crosslinking density of PP_v. Additionally, the average lamellar thickness is ~5 nm from the DSC that corresponds to 20 repeat units and much smaller than the degree of polymerization of the parent polymer (~ 93 repeat units). The sizes of network strands are thus much longer than the lamellar thickness.

Above the melting point, the linear viscoelastic spectra exhibit a modulus plateau in storage moduli, $G'(\omega)$, and a minimum in $G''(\omega)$. The appearance of the modulus plateau in $G'(\omega)$ above T_m confirms the network formation from vitrimer synthesis. However, the lack of terminal modes in these experiments (even at the highest temperature of 160 °C) prevents a clear quantification of the exchange dynamics through rheology. Furthermore, the phase separation between the PP and PEG further complicates the rheological behaviors of PP_v due to the introduction of the long-lived slow dynamics modes in the relaxation of soft domains (a leading characteristic of soft glassy materials).⁵⁹ Thus, it remains a challenge to extract the characteristics of the exchange dynamics from the rheological measurements. Nevertheless, several other features are worth noting: (i) PP vitrimers with a higher crystallinity have a higher modulus, supporting the origin of the high modulus of PP_v due to the PP crystals; (ii) a noticeable reduction of the modulus is observed for the PP vitrimers when temperature was increased from 100 °C to 120 °C, indicating a softening of the PP vitrimer upon heating. This could be due to the melting of thin lamellae of PP crystals (also note that PP_v has a relatively broad T_m window in **Figure 5**); (iii) a strong modulus reduction with increasing PEGDGE loading content is observed for both PP_v-200 and PP_v-1000; (iv) a very interesting case appeared at 130 °C, where a modulus increase emerges at the low frequencies, which is most likely due to the crystallization of PPg at 130 °C during the testing; (v) at temperatures above 130 °C, there is not too much temperature dependence of the elastic modulus for both PP_v-200 and PP_v-1000. The time-temperature superposition also fails at T > 130 °C. No terminal region can be obtained at T = 160 °C or higher. All these features further confirm the soft glassy features of the rheological spectra of PP_v with long-lived slow modes.⁵⁹ Note that the longlived slow dynamics modes often exhibit testing-time dependent properties, i.e. the aging, and leads to the failure of time-temperature superposition. 61 These characteristics are consistent with the strong structural heterogeneity and the phase separation of PP_v (Figure 7). Moreover, a nearly complete stress relaxation (Figure S15) was observed after a step strain, implying the active dynamic bond exchange in PP_v.

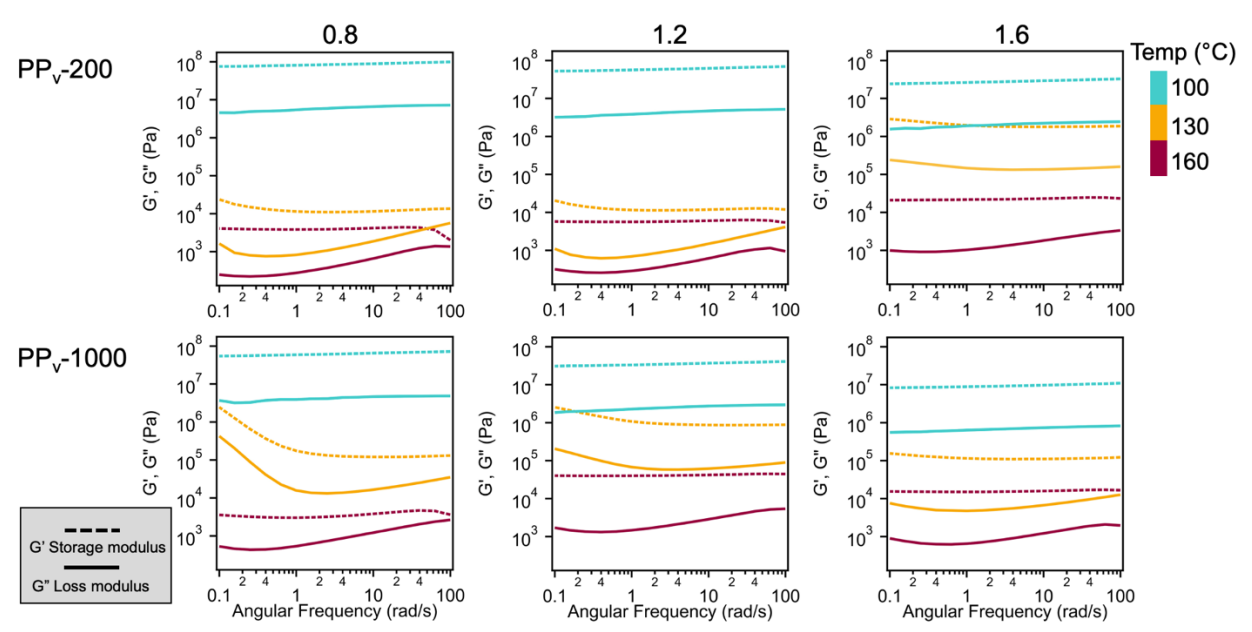


Figure 8. G' (storage modulus, dashed), and G'' (loss modulus, solid) for all PP_v samples, at 100 °C, 130 °C, and 160 °C.

Tensile deformation is applied to examine the mechanical properties of these PP_v samples as shown in Figure 9. Importantly, PPg is too brittle to prepare a thin film at room temperature (Figure 9(a)) due to their low MW and high crystallinity. As a result, the tensile properties of neat PPg is not accessible. In contrast, both PPv-200 and PPv-1000 vitrimers can form uniform films for tensile tests, suggesting a strong increase in the ductility of PP_v. As shown in Figure 9(b) and (c), the PP_v-200 vitrimers remain mostly brittle and fail at a strain of ~ 5 %, while the PP_v-1000 at PEGDGE loadings of 1.2 and 1.6 can undergo strong plastic deformation, highlighting an interesting influence of the MW of dynamic crosslinkers to the mechanical properties of PPv. The brittle nature of PP_v-200 vitrimers agrees with the general observations of poor mechanical properties of PP vitrimers with small molecule dynamic crosslinkers. Furthermore, the elastic modulus (determined from the stress ~ elongation curves) at room temperature decreases with PEGDGE content in both PP_v-200 and PP_v-1000 vitrimers, where PP_v-200 decreases from 410 MPa to 350 MPa in PP_v-200-0.8 and PP_v-200-1.2, respectively, and PP_v-1000 decreases much more, from 440 MPa (PP_v-1000-0.8) down to 140 MPa (PP_v-1000-1.6), which can be primarily attributed to the reduction in crystallinity at a higher PEG loading. Meanwhile, the ultimate tensile strength (UTS) increased significantly of the PP_v-200 and PP_v-1000 samples, where the UTS increased from 5.8 MPa (PP_v-200-0.8) up to 17.3 MPa (PP_v-1000-0.8), likely due to the formation of a stronger amorphous polymer network with higher MW polymer dynamics crosslinkers. Notably, the maximum strain of PP_v-1000 improves substantially with increasing PEGDGE content, from ~8 % for PP_v-1000-0.8 to ~37 % for PP_v-1000-1.6, which is unusual for semicrystalline polymers. Moreover, we found that the fracture energy increases dramatically from 0.06 J/m³ to 2.9 J/m³ for PP_v-200-0.8 and PP_v-1000-1.6, respectively, representing an increase of nearly 50-fold. Another nominal observation is the drastically different yielding response of the PP_v-1000-1.2 and PP_v-1000-1.6 from that of the high molecular weight PP: no stress overshoot is observed for both PP_v-1000-1.2 and PP_v-1000-1.6. Since the yielding of PP is typically due to the tilting of lamellar chain folds through a slip of the crystalline planes, 62 the lack of stress overshoot

and the weak yield stress could either be due to a reduced lamellae thickness or plastic deformation of soft domains of the structural heterogeneous vitrimers. Comparing stress-strain behaviors between PP_v-200-1.6 and PP_v-1000-1.2 further indicates that the substantially improved ductility might correlate strongly with the gel structures, as these two samples had similar gel content, yet distinct toughness and ultimate tensile strength of 0.2 J/m³, and 8.6 MPa (PP_v-200-1.6) and 2.9 J/m³ and 12.7 MPa (PP_v-1000-1.2). Additionally, the PP_v-1000-1.6 was reprocessed three times and the resulting mechanical properties as a function of recycling event are included in Figure S16. Specifically, these materials maintained a consistent UTS as the material was reprocessed three times, which were approximately 10 MPa, respectively. The elastic modulus was also slightly increases after multiple reprocessing events, from 129.2 MPa after the first cycle to 136.2 MPa after the third cycle. We also found that both PP_v-1000-1.6 and PP_v-200-1.6 exhibit strong stress relaxation after an applied step strain at 165 °C, as shown in Figure S15, which is consistent with their reversible crosslinking nature. Notably, while the physical blending of PPg and PEG1000 at a 1.2 ratio leads to similar semicrystalline morphologies, the resulting film was brittle at room temperature (this material cannot form a uniform film and therefore mechanical data is not accessible), similar to PPg, further highlighting the necessity of dynamic crosslinking to strengthen PP_v properties (Figure S17). Collectively, these results demonstrate the strong influence of polymeric crosslinkers on the gelation, morphology, and crystallization behaviors of low MW PP_g, enabling strong synergistic effects for their enhanced mechanical properties.⁵⁹

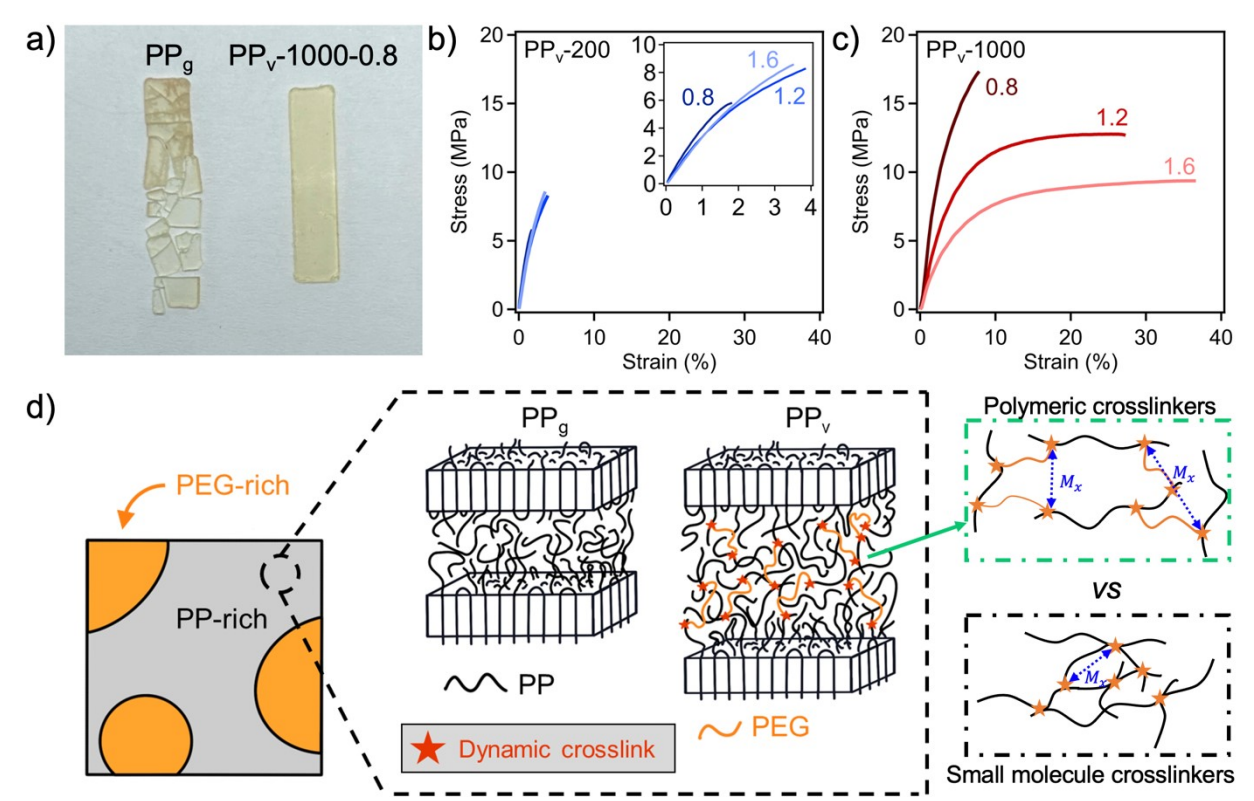


Figure 9. (a) Photo of PP_g (left) and PP_v-1000-0.8 (right) after melt pressing, showing PP_g is too fragile to remove from the mold. Stress-strain curves for (b) PP_v-200 and (c) PP_v-1000 samples were performed at the strain rate of 0.01 mm/s. (d) Schematic illustration of microphase separation of PEG and PP in vitirmers, as well as the how amorphous phase of semicrystalline PP can be

strengthened using polymeric dynamic crosslinkers, where the crosslinker is represented in orange and the dynamic crosslinking sites are shown as red stars.

3.5 Mechanism of the enhanced mechanical properties of PPv.

The above in-depth characterization of the structural and thermal, viscoelastic, and mechanical properties of PP_v highlight the important roles of polymer dynamic crosslinkers, which lead to significantly improved stretchability and toughness. While both PEG200 and PEG1000 give branching and network formation, the application of polymeric dynamic crosslinkers distinguishes this work from previous efforts focusing on small molecule counterparts, with several fundamental differences. Specifically, the use of PEG crosslinkers for polyolefin vitrimer synthesis leads to phase separation between PP and PEG phases. The dispersion of the soft PEG domains in PP matrix further toughens the obtained PP_v, in analogy to rubber toughening thermoplastics. In addition, the inclusion of polymeric crosslinkers can lead to strong modification of the crystalline microstructures of PP. It is known that the crystal size affects the mechanical properties in multiple ways. The lamellae thickness correlates the energy barrier for lamellar chain tilting at deformation. The detailed analysis of DSC results show reduction in lamellar thickness, which favors the yielding of the PP_v. The inclusion of dynamic crosslinker PEG leads to much smaller spherulites in the PP_v that dispersed in the interconnected amorphous phase (**Figure 7**), which also enhances the toughness and stretchability of the PP_v.

Lastly, the inclusion of PEG changes the polymer network structures (amorphous region), which is different from using small molecule crosslinkers: For small molecule crosslinkers, the molecular weights, M_x , between crosslinking points reduces progressively with increasing the crosslinking degree (**Figure 9d**). As a result, the strength of the network, $G \approx \frac{\rho RT}{M_x}$, increases, ⁶³ but the maximum network stretchability, $\lambda_{max} \approx \frac{N_x l}{N_x^{1/2} l} \approx N_x^{1/2} \sim M_x^{1/2}$ decreases, in which N_x is the degree of polymerization and l is the average bond length. Thus, the stretchability and ductility reduce upon the crosslinking reaction, an analogy to the well-known trade-off between modulus and stretchability in the elastomer design.⁶⁴ Note that when the polymer precursor has a low MW, high crosslinking density is required to develop a strong network. This also explains why it is so challenging to apply vitrimer chemistry to recycle low MW polyolefins. When polymer dynamic crosslinkers are employed, the M_x between the crosslink points come from two different sources: one is the PP strand between the reaction points along the PP backbone, and the other is the polymer dynamic crosslinker that does not change with the degree of crosslinking (Figure 9d). As a result, the average M_x has a much higher lower-bound even at very high crosslinking density, enabling both high strength and high stretchability of the formed network. Thus, the higher molecular weight polymer dynamics crosslinker offers a much stronger amorphous network with the simultaneous promotion of the modulus and high stretchability. The stronger amorphous network, in turn, strengthens the interplay between the amorphous region and the crystalline domain for improved ductility of the semi-crystalline polymers (Figure 9d). This explanation agrees with the observed enhancement in stretchability and toughness of PP_v-200 vitrimer than PP_g, and the much stronger ductility of PP_v-1000 vitrimer than the PP_v-200 vitrimer. It also agrees with the systematic higher shear modulus of PP_v-200 vitrimer than the PP_v-1000 at temperatures above their T_m . Thus, we attribute the combined effects of phase separation and the strong modification of the network and crystalline structures for the observed strongly enhanced mechanical properties of PP_v.

3.6. Extended value and life of PP_v in recycling.

From the above results and discussions, significantly improved mechanical properties of low MW PP (i.e., PP_g) were demonstrated, enabled by its conversion to vitrimers through chemical upcycling using polymeric crosslinkers. In this section, we demonstrate an immediate application of the obtained PP_v through their blending with PP_h (Figure 10(a)). Noteworthily, multiple states, including California, Washington, Oregon, and New Jersey, have recently implemented the mandated use of PCR in manufacturing new products. These requirements have started at levels between 10-15 wt% and plan to increase up to 50 wt% by 2031,65 requiring new design for the strategic use of plastic waste-derived chemicals. In response to these government mandates and policies, we studied the mechanical properties of commodity PP_h blended with 15 wt% of PP_v-1000-1.6. The neat PP_h and a blend of PP_h with 15 wt% of PP_g were also tested as references. Figure 10(b, c) compares the tensile properties of these three samples. The neat PPh undergoes normal yielding, strain softening, necking and necking propagation, and strain hardening before the final fracture (the black line), while the PP_h/PP_g blend only shows yielding and strain softening, and cannot undergo necking propagation. Specifically, PP_h/PP_g has a low elongation-at-break of only ~50 %. From SAXS results (Figure S18b), it was found that the PPh/PPg blend can form two types of lamellar crystals with a distinct long period, d, at 16 nm and 7 nm respectively. This result can be used to explain why blending 15 wt% PPg can be very detrimental in waste recycling systems, as they create defective sites due to insufficient amount of tie chains. As a comparison, PPh/PPv-1000-1.6 showed comparable mechanical responses to neat PPh, including yielding, necking, and even strain-hardening behaviors. The UTS was 26.3 MPa and 22.6 MPa for PPh and PPh/PPv-1000-1.6, respectively, while the elongation for the materials decreased slightly from 1167 % for neat PP_h to 1045 % for the PP_h/PP_v-1000-1.6 blend, suggesting their comparable mechanical properties (Figure 10(c)). These results further confirm that PP_v samples have the necessary processability and properties for their extended use and lifetime. Interestingly, SAXS measurements of neat PPh, PPh/PPg blends (15 wt% PPg), and PPh/PPv blends (15 wt%) show no signs of large-scale phase separation in these samples. In addition, the POM measurements (Figure S19) show similar crystalline morphology of PP_h and the PP_h/PP_v-1000-1.6 at isothermal crystallization conditions at 125 °C. Noticeable heterogeneities in crystallization and crystal growth are also absence. Thus, both the SAXS measurements and the POM measurements indicate good dispersions of PP_v-1000-1.6 in PP_h and the significant role of PP_v network for the toughening of PP_b/PP_v blends. Therefore, our work demonstrates an important new system design, including the conversion of PPg to PPv using polymeric crosslinkers and blending them into PPh, which could provide a more sustainable solution for building up plastic circularity, ⁶⁶ while addressing the need for remediating waste plastic by enabling their use as feedstock materials.

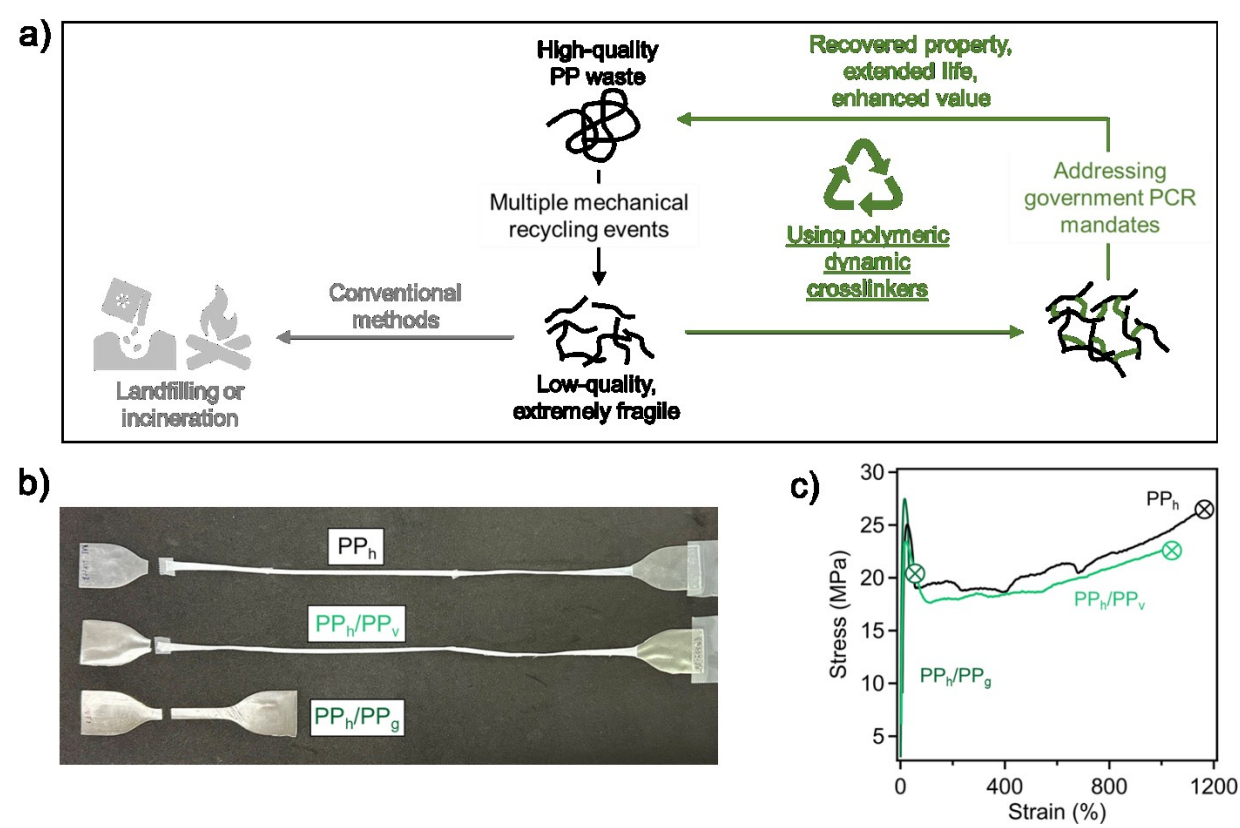


Figure 10. (a) Alternative route for recycling low-quality PP in order to enable a closed-loop material stream. (b) fractured tensile bars for PP_h (black), PP_h/PP_v-1000-1.6 (light green), and PP_h/PP_g (dark green), and (c) Stress-strain curves and performed at 5 mm/min.

4. Conclusions

In this work, we have demonstrated a successful and scalable strategy to convert low MW PP to vitrimers with substantially enhanced mechanical properties using polymeric dynamic crosslinkers, which cannot be achieved through employing small molecule counterparts. In particular, the polymeric crosslinkers can introduce soft domains to toughening the network, alter the crystallinity and morphology of PP, and strengthen the network structures in a way that is fundamentally different from their small molecule crosslinkers. As a result, the obtained new types of PP vitrimers can have greatly improved thermal stability and mechanical properties than the virgin low MW PP. To demonstrate the practical application of the obtained PP_v as additives, we further characterize the mechanical properties of PPh/PPv blends with up to 15 wt% PPv content, which provides mechanical properties comparable to that of neat commodity PPh, including toughness and elongation. These promising results thus demonstrate a working strategy towards addressing low MW, "no-value" PP for establishing a circular economy for plastics. Since the revealed molecular mechanisms are not limited to PP, we anticipate the reported strategy can be generalized and broadly employed for polyolefin upcycling or other semi-crystalline polymers, especially the low MW wastes, through incorporating polymeric dynamic crosslinkers. However, we also would like to point out that the introduction of PEG into waste PP stream may not be desired as it can create an additional layer of complexity for waste management. Nevertheless, the use of polymeric dynamic crosslinker for upcycling of polyolefin wastes should be further investigated as a potential strategy to enable value-added products with controlled mechanical properties. Future opportunities might exist to identify bio-degradable polymers as the crosslinkers and understand the impact of crosslinker chemistry, composition and topology on controlling the crystallization behaviors and mechanical properties of polyolefin vitrimers.

5. Acknowledgements

This work was partially supported by National Science Foundation Office of Integrative Activities #2132144. ZQ would also like to acknowledge financial support provided from ACS Petroleum Research Fund (award no. 65268-DNI7). S.C. acknowledges the support from National Science Foundation with the Award number NSF-DMR 2211573. The SAXS measurements were performed at Beamline 12-ID-B of Advanced Photon Source with the help of Dr. Xiaobing Zuo, a U.S. Department of Energy (DOE) Office of Science User Facility operated for the DOE Office of Science by Argonne National Laboratory under Contract No. DE-AC-0206CH11357.

6. Associated Content

Supporting information includes the following data: Force versus time plot of compounding reaction; comparison of reaction with and without catalyst; enlarged FT-IR spectrum for PP_v-200 series; TGA thermograms; T_c for both PP_v-200 and PP_v-1000 materials; DSC heating and cooling thermograms for PEG200 and PEG1000; degree of crystallinity; lamellar thickness distributions for PP_g and PP_v materials; log-log SAXS plots and WAXS diffractograms with labeled planes; SEM image of PP_v-1000-1.6; Rheological testing data including SAOS with full temperature range, and stress relaxation; mechanical properties of PP_v after multiple reprocessing events, WAXS and SAXS plots for PP_h blends; photo of melt pressed sample, DSC thermogram, and SAXS data of PP_g/PEG900; and tables including sample names, contents, reaction conditions, as well as the melting temperature, crystallinity, lamellar thickness, and long period of each material.

This material is available free of charge via the Internet at http://pubs.acs.org.

7. Author Information

Corresponding Authors:

Shiwang Cheng (S.C. Email: chengsh9@msu.edu) and Zhe Qiang (Z.Q. Email: zhe.qiang@usm.edu)

Author Contributions:

The manuscript was written through contributions of all authors. *M. S and *S. P contributed equally to this project.

8. Notes

The authors have no competing financial interests.

References

- (1) Allahvaisi, S. Polypropylene in the Industry of Food Packaging. In *Polypropylene*; Dogan, F., Ed.; 2012; pp 1–20.
- (2) Nguyen, H. L.; Tran, T. H.; Hao, L. T.; Jeon, H.; Koo, J. M.; Shin, G.; Hwang, D. S.; Hwang, S. Y.; Park, J.; Oh, D. X. Biorenewable, Transparent, and Oxygen/Moisture Barrier Nanocellulose/Nanochitin-Based Coating on Polypropylene for Food Packaging Applications. *Carbohydr. Polym.* **2021**, *271*, 118421. DOI: 10.1016/j.carbpol.2021.118421
- (3) Dopico-García, M. S.; López-Vilariñó, J. M.; González-Rodríguez, M. v. Antioxidant Content of and Migration from Commercial Polyethylene, Polypropylene, and Polyvinyl Chloride Packages. *J. Agric. Food Chem.* **2007**, *55* (8), 3225–3231. DOI: 10.1021/jf070102+
- (4) Hufenbach, W.; Böhm, R.; Thieme, M.; Winkler, A.; Mäder, E.; Rausch, J.; Schade, M. Polypropylene/Glass Fibre 3D-Textile Reinforced Composites for Automotive Applications. *Mater. Des.* **2011**, *32* (3), 1468–1476. DOI: 10.1016/j.matdes.2010.08.049
- (5) Gai, K.; Ren, X.; Chen, J.; Zhou, X.; Wan, Q.; Wang, Q.; Li, Y. Construction of Helically Oriented Syndiotactic Polypropylene/Isotactic Polypropylene Composites for Medical Interventional Tubes via Rotation Extrusion. *Ind. Eng. Chem. Res.* **2023**, 62 (2), 971-981. DOI: 10.1021/acs.iecr.2c03446.
- (6) Corrêa, H. L.; Corrêa, D. G. Polymer Applications for Medical Care in the COVID-19 Pandemic Crisis: Will We Still Speak Ill of These Materials? *Front. Mater.* **2020**, 7 (August), 1–6. DOI: 10.3389/fmats.2020.00283
- (7) Plastics Europe. *Plastics the Facts 2022*; 2022. https://plasticseurope.org/knowledge-hub/plastics-the-facts-2022/. Accessed on 2/1/2023
- (8) Jiang, J. Q. Occurrence of Microplastics and Its Pollution in the Environment: A Review. *Sustain. Prod. Consum.* **2018**, *13* (November), 16–23. DOI: 10.1016/j.spc.2017.11.003
- (9) Prata, J. C.; da Costa, J. P.; Lopes, I.; Duarte, A. C.; Rocha-Santos, T. Environmental Exposure to Microplastics: An Overview on Possible Human Health Effects. *Sci. Total Environ.* **2020**, *702*, 134455. DOI: 10.1016/j.scitotenv.2019.134455
- (10) Tang, C. C.; Chen, H. I.; Brimblecombe, P.; Lee, C. L. Morphology and Chemical Properties of Polypropylene Pellets Degraded in Simulated Terrestrial and Marine Environments. *Mar. Pollut. Bull.* **2019**, *149* (October), 110626. DOI: 10.1016/j.marpolbul.2019.110626
- (11) Jehanno, C.; Alty, J. W.; Roosen, M.; de Meester, S.; Dove, A. P.; Chen, E. Y. X.; Leibfarth, F. A.; Sardon, H. Critical Advances and Future Opportunities in Upcycling Commodity Polymers. *Nature* **2022**, *603* (7903), 803–814. DOI: 10.1038/s41586-021-04350-0

- (12) Roy, P. S.; Garnier, G.; Allais, F.; Saito, K. Strategic Approach Towards Plastic Waste Valorization: Challenges and Promising Chemical Upcycling Possibilities. *ChemSusChem* **2021**, *14* (19), 4007–4027. DOI: 10.1002/cssc.202100904
- (13) Xanthos, M. Recycling of the #5 Polymer. *Science* (1979) **2012**, 337 (6095), 700–702. DOI: 10.1126/science.1221806
- (14) Yin, S.; Tuladhar, R.; Shi, F.; Shanks, R. A.; Combe, M.; Collister, T. Mechanical Reprocessing of Polyolefin Waste: A Review. *Polym. Eng. Sci.* **2015**, *55* (12), 2899–2909. DOI: 10.1002/pen.24182
- (15) da Costa, H. M.; Ramos, V. D.; de Oliveira, M. G. Degradation of Polypropylene (PP) during Multiple Extrusions: Thermal Analysis, Mechanical Properties and Analysis of Variance. *Polym. Test* **2007**, *26* (5), 676–684. DOI: 10.1016/j.polymertesting.2007.04.003
- (16) Fazekas, T. J.; Alty, J. W.; Neidhart, E. K.; Miller, A. S.; Leibfarth, F. A.; Alexanian, E. J. Diversification of Aliphatic C-H Bonds in Small Molecules and Polyolefins through Radical Chain Transfer. *Science* **2022**, *375* (6580), 545–550. DOI: 10.1126/science.abh4308
- (17) Samanta, S.; Kim, S.; Saito, T.; Sokolov, A. P. Polymers with Dynamic Bonds: Adaptive Functional Materials for a Sustainable Future. *J. Phys. Chem. B* **2021**, *125* (33), 9389–9401. DOI: 10.1021/acs.jpcb.1c03511
- (18) Kar, G. P.; Saed, M. O.; Terentjev, E. M. Scalable Upcycling of Thermoplastic Polyolefins into Vitrimers through Transesterification. J. Mater. Chem. A. 2020, 8 (45), 24137–24147. DOI: 10.1039/D0TA07339C
- (19) Ji, F.; Liu, X.; Sheng, D.; Yang, Y. Epoxy-Vitrimer Composites Based on Exchangeable Aromatic Disulfide Bonds: Reprocessibility, Adhesive, Multi-Shape Memory Effect. *Polymer* **2020**, *197* (February), 122514. DOI: 10.1016/j.polymer.2020.122514
- (20) Huang, J.; Gong, Z.; Chen, Y. A Stretchable Elastomer with Recyclability and Shape Memory Assisted Self-Healing Capabilities Based on Dynamic Disulfide Bonds. *Polymer* **2022**, *242*. DOI: 10.1016/j.polymer.2022.124569
- (21) Fenimore, L. M.; Chen, B.; Torkelson, J. M. Simple Upcycling of Virgin and Waste Polyethylene into Covalent Adaptable Networks: Catalyst-Free, Radical-Based Reactive Processing with Dialkylamino Disulfide Bonds. *J. Mater. Chem. A.* **2022**, 24726–24745. DOI: 10.1039/d2ta06364f
- (22) He, Z.; Niu, H.; Liu, L.; Xie, S.; Hua, Z.; Li, Y. Elastomeric Polyolefin Vitrimer: Dynamic Imine Bond Cross-Linked Ethylene/Propylene Copolymer. *Polymer* **2021**, *229* (July), 124015. DOI: 10.1016/j.polymer.2021.124015
- (23) Yang, Y.; Huang, L.; Wu, R.; Niu, Z.; Fan, W.; Dai, Q.; Cui, L.; He, J.; Bai, C. Self-Strengthening, Self-Welding, Shape Memory, and Recyclable Polybutadiene-Based

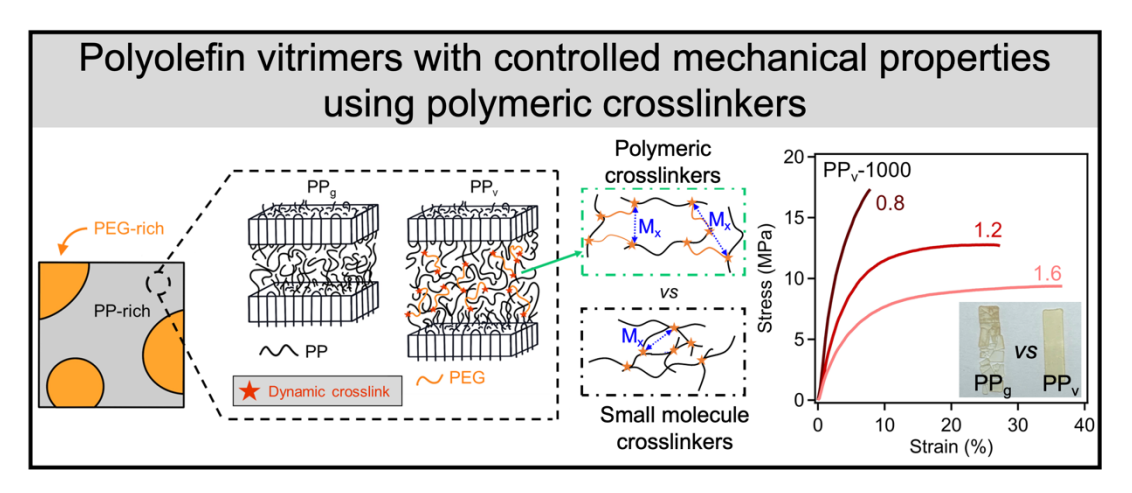
- Material Driven by Dual-Dynamic Units. ACS Appl. Mater. Interfaces **2022**, 14 (2), 3344–3355. DOI: 10.1021/acsami.1c23007
- (24) Saed, M. O.; Lin, X.; Terentjev, E. M. Dynamic Semicrystalline Networks of Polypropylene with Thiol-Anhydride Exchangeable Crosslinks. *ACS Appl. Mater. Interfaces* **2021**, *13* (35), 42044–42051. DOI: 10.1021/acsami.1c12099
- (25) Tretbar, C. A.; Neal, J. A.; Guan, Z. Direct Silyl Ether Metathesis for Vitrimers with Exceptional Thermal Stability. *J. Am. Chem. Soc.* **2019**, *141* (42), 16595–16599. DOI: 10.1021/jacs.9b08876
- (26) Zych, A.; Pinalli, R.; Soliman, M.; Vachon, J.; Dalcanale, E. Polyethylene Vitrimers via Silyl Ether Exchange Reaction. *Polymer* **2020**, *199* (February). DOI: 10.1016/j.polymer.2020.122567
- (27) Röttger, M.; Domenech, T.; van der Weegen, R.; Breuillac, A.; Nicolaÿ, R.; Leibler, L. High-Performance Vitrimers from Commodity Thermoplastics through Dioxaborolane Metathesis. *Science* **2017**, *356* (6333), 62–65. DOI: 10.1126/science.aah5281
- (28) Xiao, Y.; Liu, P.; Wang, W. J.; Li, B. G. Dynamically Cross-Linked Polyolefin Elastomers with Highly Improved Mechanical and Thermal Performance. *Macromolecules* **2021**, *54* (22), 10381–10387. DOI: 10.1021/acs.macromol.1c01249
- (29) Soman, B.; Schweizer, K. S.; Evans, C. M. Fragile Glass Formation and Non-Arrhenius Upturns in Ethylene Vitrimers Revealed by Dielectric Spectroscopy. *Macromolecules* **2023**, 56 (1), 166–176. DOI: 10.1021/acs.macromol.2c01657
- (30) Ahmadi, M.; Hanifpour, A.; Ghiassinejad, S.; van Ruymbeke, E. Polyolefins Vitrimers: Design Principles and Applications. *Chem. Mater.* **2022**, *34* (23), 10249–10271. DOI: 10.1021/acs.chemmater.2c02853
- (31) Maaz, M.; Riba-Bremerch, A.; Guibert, C.; van Zee, N. J.; Nicolaÿ, R. Synthesis of Polyethylene Vitrimers in a Single Step: Consequences of Graft Structure, Reactive Extrusion Conditions, and Processing Aids. *Macromolecules* **2021**, *54* (5), 2213–2225. DOI: 10.1021/acs.macromol.0c02649
- (32) Peng, L. M.; Xu, Z.; Wang, W. Y.; Zhao, X.; Bao, R. Y.; Bai, L.; Ke, K.; Liu, Z. Y.; Yang, M. B.; Yang, W. Leakage-Proof and Malleable Polyethylene Wax Vitrimer Phase Change Materials for Thermal Interface Management. *ACS Appl. Energy. Mater.* **2021**, *4* (10), 11173–11182. DOI: 10.1021/acsaem.1c02052
- (33) Soman, B.; Go, Y. K.; Shen, C.; Leal, C.; Evans, C. M. Impact of Dynamic Covalent Chemistry and Precise Linker Length on Crystallization Kinetics and Morphology in Ethylene Vitrimers. *Soft Matter* **2022**, *18* (2), 293–303. DOI: 10.1039/D1SM01288F
- (34) Ji, F.; Liu, X.; Lin, C.; Zhou, Y.; Dong, L.; Xu, S.; Sheng, D.; Yang, Y. Reprocessable and Recyclable Crosslinked Polyethylene with Triple Shape Memory Effect. *Macromol. Mater. Eng.* **2019**, *304* (3), 1–8. DOI: 10.1002/mame.201800528

- (35) Korley, L. T. J.; Epps, T. H.; Helms, B. A.; Ryan, A. J. Toward Polymer Upcycling—Adding Value and Tackling Circularity. *Science* **2021**, *373* (6550), 66–69. DOI: 10.1126/science.abg4503
- (36) Epps, T. H.; Korley, L. T. J.; Yan, T.; Beers, K. L.; Burt, T. M. Sustainability of Synthetic Plastics: Considerations in Materials Life-Cycle Management. *JACS Au* **2022**, *2* (1), 3–11. DOI: 10.1021/jacsau.1c00191
- (37) Almeida, S.; Raposo, A.; Almeida-González, M.; Carrascosa, C. Bisphenol A: Food Exposure and Impact on Human Health. *Compr. Rev. Food Sci. Food Saf.* **2018**, *17* (6), 1503–1517. DOI: 10.1111/1541-4337.12388
- (38) Kadasala, N. R.; Narayanan, B.; Liu, Y. International Trade Regulations on BPA: Global Health and Economic Implications. *Asian Dev. Policy Rev.* **2016**, *4* (4), 134–142. DOI: 10.18488/journal.107/2016.4.4/107.4.134.142
- (39) Xu, Z.; Sun, R.; Lu, W.; Patil, S.; Mays, J.; Schweizer, K. S.; Cheng, S Nature of Steady-State Fast Flow in Entangled Polymer Melts: Chain Stretching, Shear Thinning, and Viscosity Scaling. *Macromolecules*. **2022**, *55* (23), 10737-10750. DOI: 10.1021/acs.macromol.2c01345
- (40) Capelot, M.; Montarnal, D.; Tournilhac, F.; Leibler, L. Metal-Catalyzed Transesterification for Healing and Assembling of Thermosets. *J. Am. Chem. Soc.* **2012**, *134* (18), 7664–7667. DOI: 10.1021/ja302894k
- (41) Krishnakumar, B.; Sanka, R. V. S. P.; Binder, W. H.; Parthasarthy, V.; Rana, S.; Karak, N. Vitrimers: Associative Dynamic Covalent Adaptive Networks in Thermoset Polymers. *Chem. Eng. J.* **2020**, *385* (July), 123820. DOI: 10.1016/j.cej.2019.123820
- (42) Chan, J. H.; Balke, S. T. The Thermal Degradation Kinetics of Polypropylene: Part III. Thermogravimetric Analyses. *Polym. Degrad. Stab.* **1997**, *57* (2), 135–149. DOI: 10.1016/S0141-3910(96)00160-7
- (43) Calahorra, M. E.; Cortázar, M.; Eguiazábal, J. I.; Guzmán, G. M. Thermogravimetric Analysis of Cellulose: Effect of the Molecular Weight on Thermal Decomposition. *J. Appl. Polym. Sci.* **1989**, *37* (12), 3305–3314. DOI: 10.1002/app.1989.070371203
- (44) Onuki, A. Phase transitions of fluids in shear flow. *J. Phys. Condens. Matter* **1997**, 9 (29), 6119-6157.
- (45) Tanaka, H.; Araki, T. Viscoelastic phase separation in soft matter: Numerical-simulation study on its physical mechanism. *Chem. Eng. Sci.* **2006**, 61 (7), 2108-2141.
- (46) Chen, H.; Shi, X.; Zhu, Y.; Zhang, Y.; Xu, J. Surface Modification of Polypropylene. I. Surface Enrichment of Poly(Ethylene Glycol) on Polypropylene/Poly(Ethylene Glycol) Blends. *J. Vinyl Addit. Technol.* **2008**, *14* (1), 28–33. DOI: 10.1002/vnl.20140.

- (47) Chen, Q. P.; Xie, S.; Foudazi, R.; Lodge, T. P.; Siepmann, J. I. Understanding the Molecular Weight Dependence of χ and the Effect of Dispersity on Polymer Blend Phase Diagrams. *Macromolecules* **2018**, 51 (10), 3774-3787.
- (48) Khonakdar, H. A.; Morshedian, J.; Wagenknecht, U.; Jafari, S. H. An Investigation of Chemical Crosslinking Effect on Properties of High-Density Polyethylene. *Polymer* 2003, 44 (15), 4301–4309. DOI: 10.1016/S0032-3861(03)00363-X
- (49) Krumova, M.; López, D.; Benavente, R.; Mijangos, C.; Pereña, J. M. Effect of Crosslinking on the Mechanical and Thermal Properties of Poly(Vinyl Alcohol). *Polymer* **2000**, *41* (26), 9265–9272. DOI: 10.1016/S0032-3861(00)00287-1
- (50) Rozanski, A.; Safandowska, M.; Krajenta, A. DSC/SAXS Analysis of the Thickness of Lamellae of Semicrystalline Polymers-Restrictions in the Case of Materials with Swollen Amorphous Phase. *Polym. Test* **2018**, *65* (December), 189–196. DOI: 10.1016/j.polymertesting.2017.11.028
- (51) Monasse, B.; Haudin, J. M. Growth Transition and Morphology Change in Polypropylene. *Colloid Polym. Sci.* **1985**, *263* (10), 822–831. DOI: 10.1007/BF01412960
- (52) Kang, J.; Chen, J.; Cao, Y.; Li, H. Effects of Ultrasound on the Conformation and Crystallization Behavior of Isotactic Polypropylene and β-Isotactic Polypropylene. *Polymer* **2010**, *51* (1), 249–256. DOI: 10.1016/j.polymer.2009.11.018
- (53) Ahmadi, M.; Mortazavi, S. M. M.; Ahmadjo, S.; Zahamti, M.; Valieghbal, K.; Jafarifar, D.; Rashedi, R. Evaluation of Continuous and Discrete Melting Endotherms for Determination of Structural Heterogeneities in Ziegler-Natta Catalyzed Linear Low Density Polyethylene *Polyolefin Journals* **2016**, *3* (2), 135-146
- (54) Polińska, M.; Rozanski, A.; Galeski, A.; Bojda, J. The Modulus of the Amorphous Phase of Semicrystalline Polymers. *Macromolecules* **2021**, *54* (19), 9113–9123. DOI: 10.1021/acs.macromol.1c01576
- (55) Cheng, S. Z. D.; Janimak, J. J.; Zhang, A.; Hsieh, E. T. Isotacticity Effect on Crystallization and Melting in Polypropylene Fractions: 1. Crystalline Structures and Thermodynamic Property Changes. *Polymer* **1991**, *32* (4), 648–655. DOI: 10.1016/0032-3861(91)90477-Z
- (56) Feng, J.; Chen, M. Effects of La3+-Containing Additive on Crystalline Characteristics of Isotactic Polypropylene. *Polym. Int.* **2003**, *52* (1), 42–45. DOI: 10.1002/pi.984
- (57) Ou, C. F. The Crystallization Characteristics of Polypropylene and Low Ethylene Content Polypropylene Copolymer with Copolyesters. *Eur. Polym. J.* **2002**, *38* (3), 467–473. DOI: 10.1016/S0014-3057(01)00218-X
- (58) Mileva, D.; Tranchida, D.; Gahleitner, M. Designing Polymer Crystallinity: An Industrial Perspective. *Polym. Crystallization* **2018**, *I* (2), 1–16. DOI: 10.1002/pcr2.10009
- (59) Sollich, P. Rheological constitutive equation for a model of soft glassy materials. Phys. Rev. E 1998, 58 (1), 738-759

- (60) Fetters, L. J.; Lohse, D. J.; Richter, D.; Witten, T. A.; Zirkel, A. Connection between polymer molecular weight, density, chain dimensions, and melt viscoelastic properties. *Macromolecules* **1994**, 27 (17), 4639-4647.
- (61) Fielding, S. M.; Sollich, P.; Cates, M. E. Aging and rheology in soft materials. *J. Rheol.* **2000**, 44 (2), 323-369.
- (62) Baltá-Calleja, F. J.; Peterlin, A. Plastic Deformation of Polypropylene. VI. Mechanism and Properties. *J. Macromol. Sci. B* **1970**, *4* (3), 519–540. DOI: 10.1080/00222347008229372
- (63) Treloar, L. R. G. The Physics of Rubber Elasticity, 3rd ed.; Oxford, 2005.
- (64) Lake, G. J.; Thomas, A. G. The strength of highly elastic materials. *Proc. R. Soc. London, Ser. A* **1967**, *300* (1460), 108-119. DOI: 10.1098/rspa.1967.0160
- (65) Irby, C. Recycling Regulations for Plastic Packaging in the United States. Plascene. https://www.plascene.com/recycling-regulations-for-plastic-packaging-in-the-united-states (accessed 2023-01-21).
- (66) Iacovidou, E.; Geyer, R.; Kalow, J.; Palardy, J.; Dunn, J.; Hoellein, T.; Xiong, B.; Chen, E. Y. X. Toward a Circular Economy for Plastics. *One Earth* 2021, 4 (5), 591–594. DOI: 10.1016/j.oneear.2021.04.023

TOC Figure



Supporting Information:

Polymeric Dynamic Crosslinker for Upcycling of Fragile Low Molecular Weight Polypropylene

Mikaela Sadri^{1, #}, Shalin Patil^{2, #}, Jonathan Perkins¹, Zoe Gunter¹, Shiwang Cheng^{2,*}, Zhe Qiang^{1,*}

¹School of Polymer Science and Engineering, The University of Southern Mississippi, Hattiesburg, MS, US, 39406

Correspondence to: S. C. (Email: chengsh9@msu.edu); Z. Q. (Email: <u>zhe.qiang@usm.edu</u>) *M. S and *S. P contributed equally to this project.

²Department of Chemical Engineering and Materials Science, Michigan State University, East Lansing, MI, US, 48864

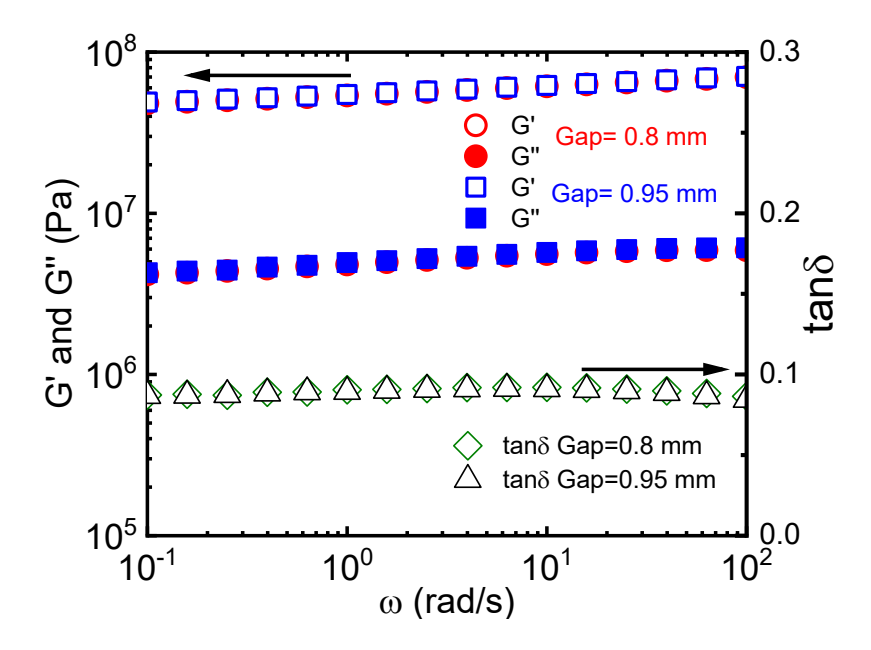


Figure S1. Small amplitude oscillatory shear measurements of PPv-1000-1.6 at 80 °C for two different gaps of 0.95 mm and 0.80 mm. The excellent agreement in the storage modulus, G', the loss modulus, G'', and the loss factor, $tan\delta$, suggests the absence of shear detachment or wall slip in the measurements.

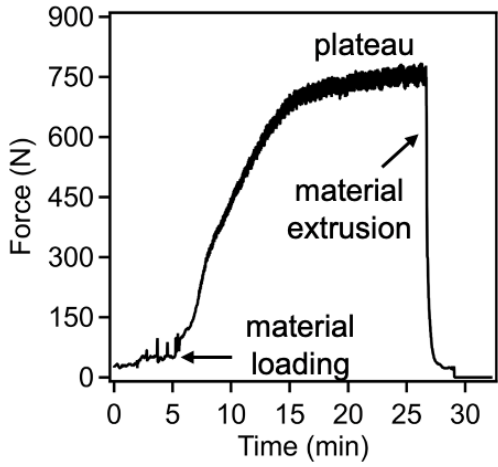


Figure S2. Force as a function of time during the epoxy-anhydride curing process as determined by the sensors in microcompounder. Sample shown in the Figure is PP_v-1000-1.2.

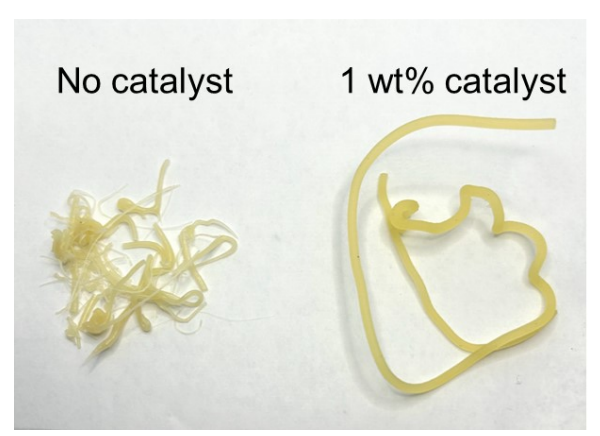


Figure S3. Photos of extruded PP samples crosslinked by PEGDGE1000 at 1.6 with and without the presence of Zn(acac)₂ catalyst.

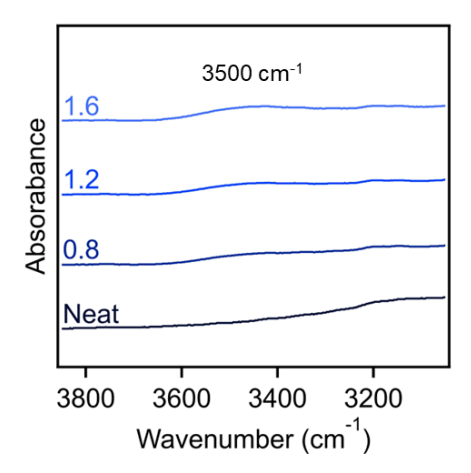


Figure S4. FT-IR spectrum of PP_g and PP_v -200 vitrimers, at a selected wavenumber range corresponding to the O-H stretching.

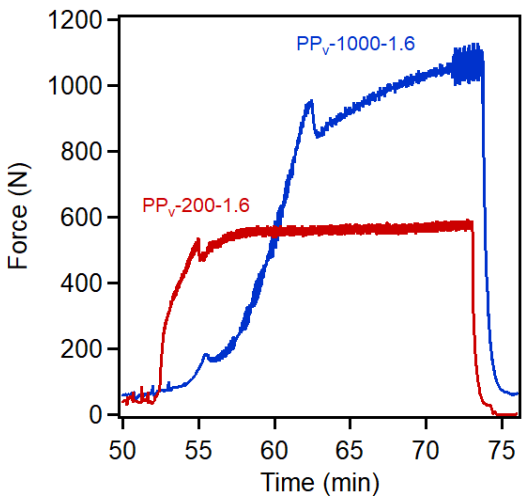


Figure S5. Force as a function of time during the epoxy-anhydride curing process as determined by the sensors in a microcompounder for samples PP_v -200-1.6 (red) and PP_v -1000-1.6 (blue).

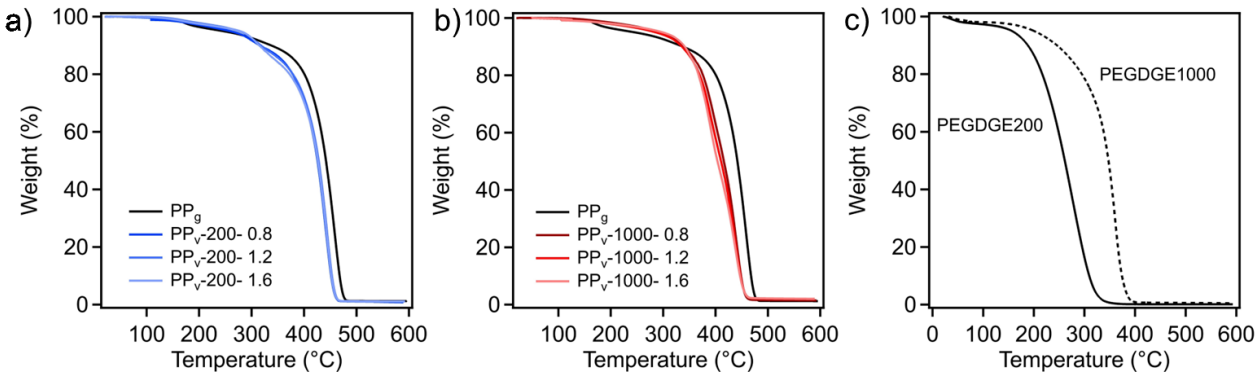


Figure S6. TGA curves in nitrogen for (a) PP_v-200 vitrimers, (b) PP_v-1000 vitrimers, and (c) PEG200 (solid) and PEG1000 (dashed) at a heating rate of 10 °C/min.

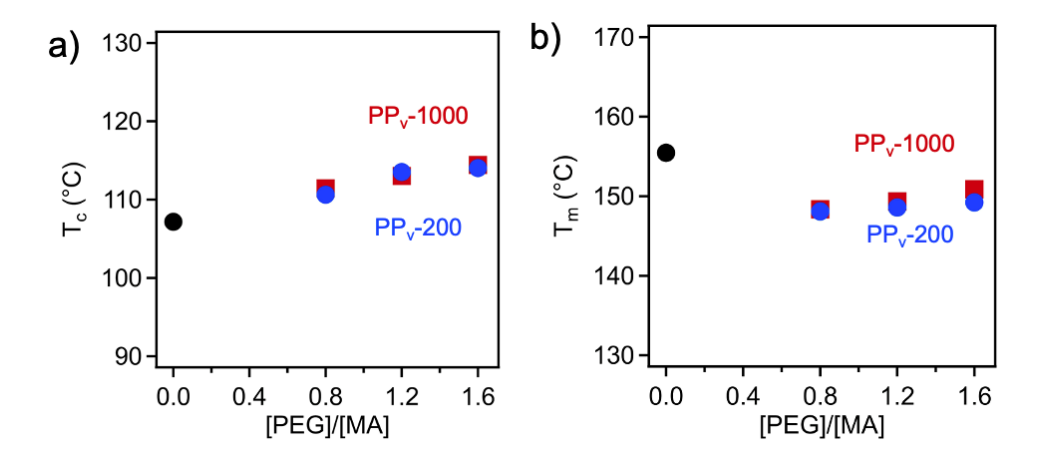


Figure S7. (a) T_c and (b) T_m of PP_g (black circle), PP_v-200 vitrimers (blue circles), and PP_v-1000 vitrimers (red squares) with varied crosslinker content.

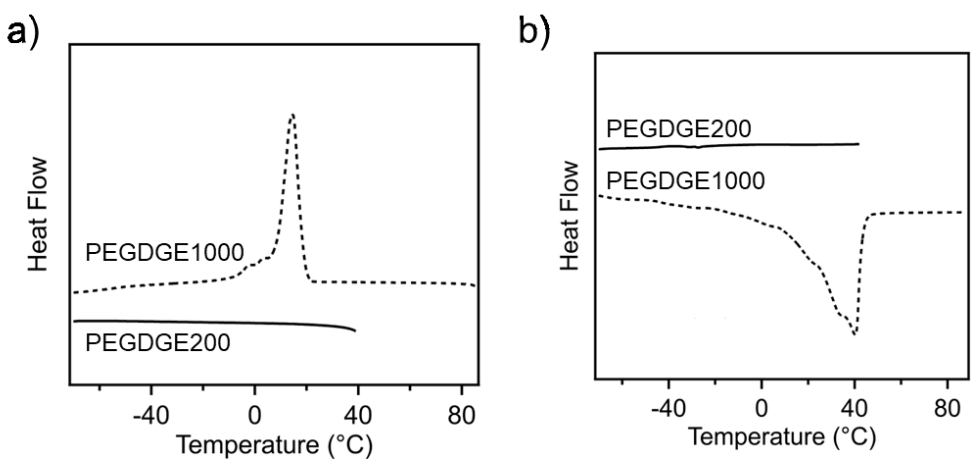


Figure S8. DSC curves for showing the a) cooling and b) heating steps of neat PEG200 (solid) and PEG1000 (dashed) at a ramp rate of 10 °C/min.

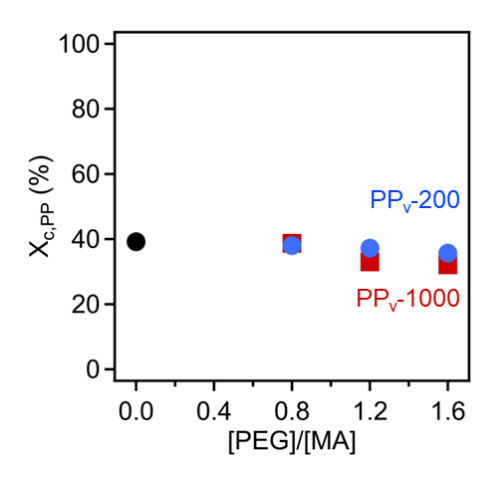


Figure S9. Degree of crystallinity in the PP domain for PP_g and PP_v samples.

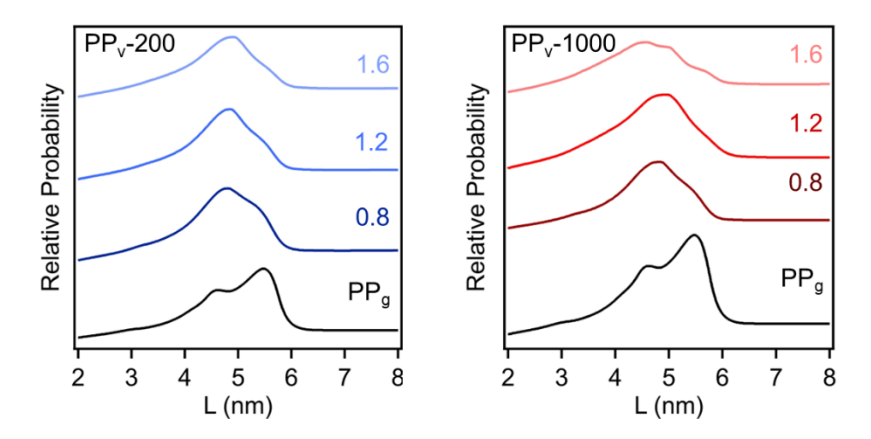


Figure S10. Lamellar thickness distribution for PP_v-200 (left) and PP_v-1000 (right) samples.

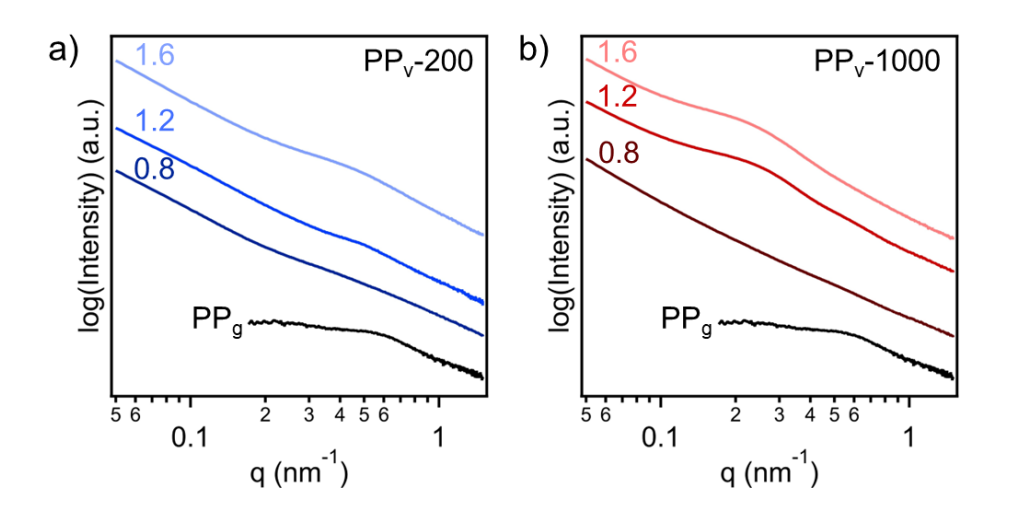


Figure S11. SAXS plot of a) PP_v-200 and b) PP_v-1000 vitrimers.

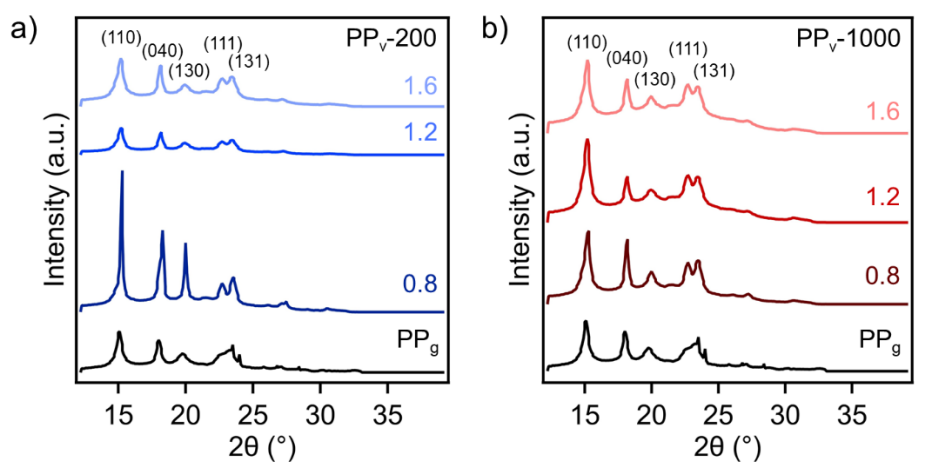


Figure S12. WAXS plot of a) PP_v-200 and b) PP_v-1000 samples, with labeled planes.

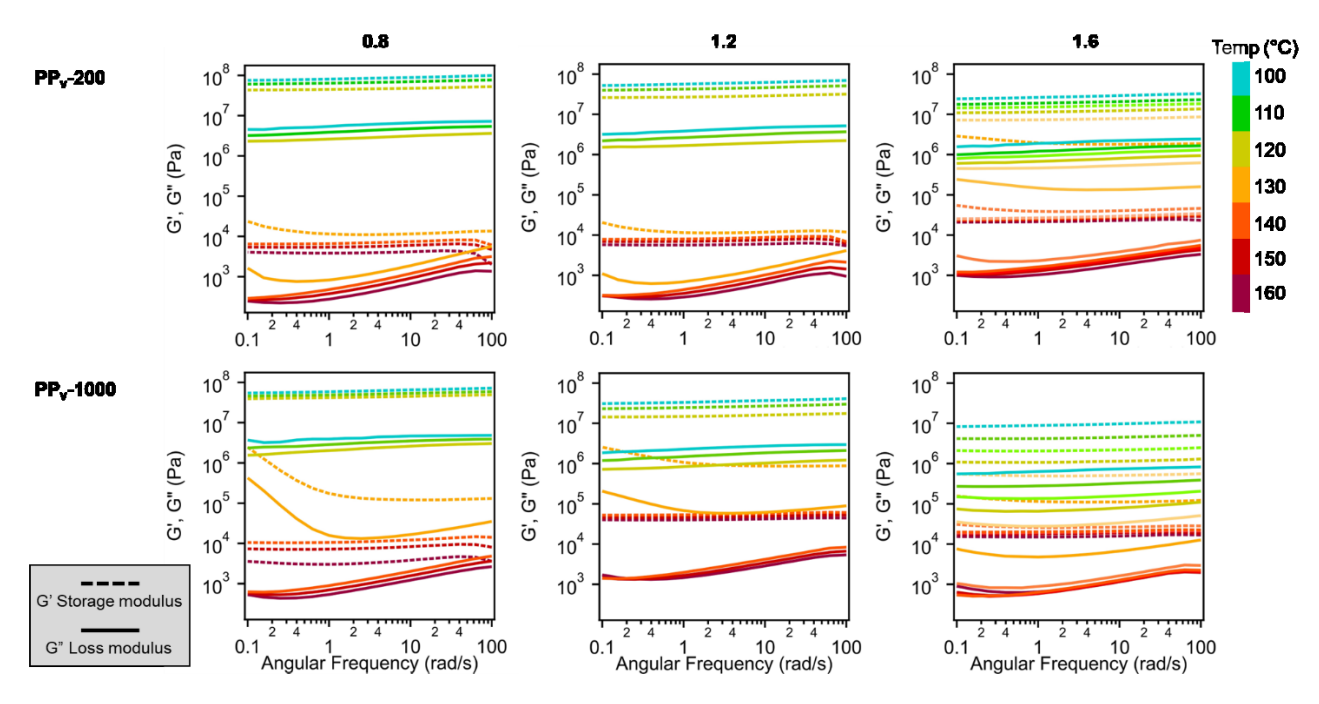


Figure S13. Storage and loss modulii of PP_v -200 (top row) and PP_v -1000 (bottom row) vitrimers every 10 degrees ranging from 100 °C to 160 °C via SAOS measurements.

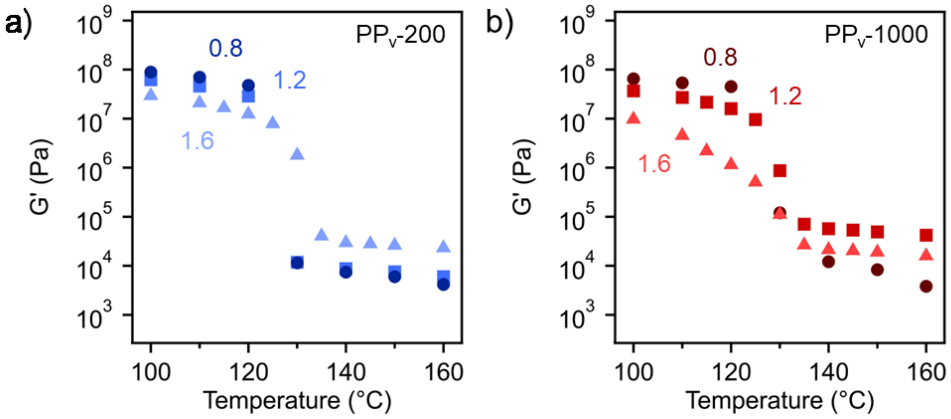


Figure S14. Storage modulus across temperatures at 10 rad/s for a) PPv-200 and b) PPv-1000, extracted from SAOS measurements.

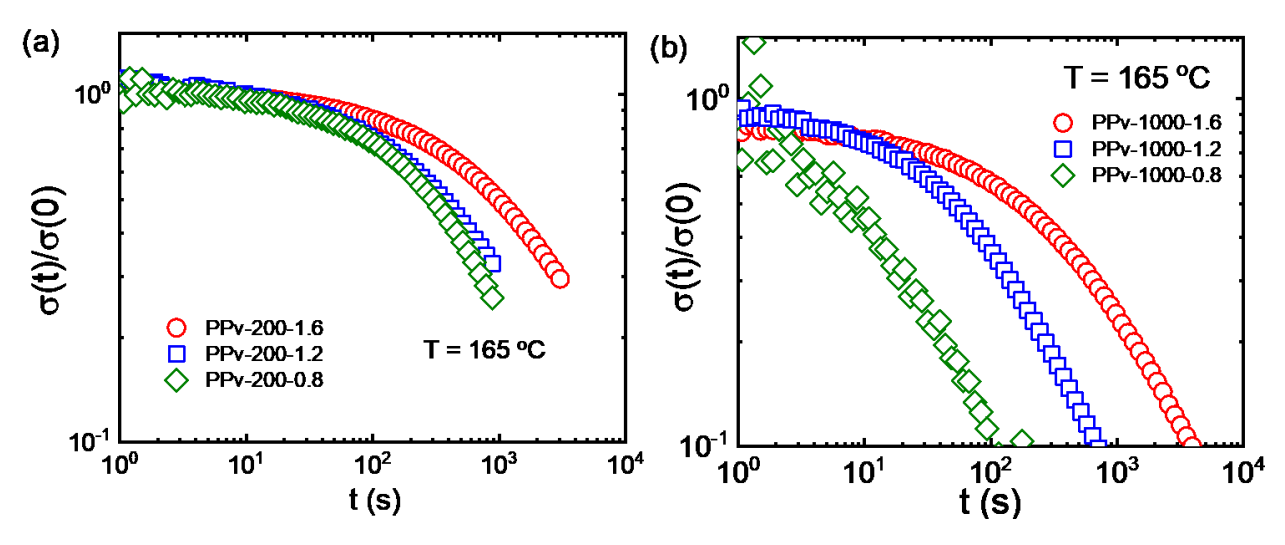


Figure S15. Stress relaxation after a step-strain of (a) PP_v -200 vitrimers and (b) PP_v -1000 vitrimers. The strain is 5% and the strain rate is 0.01 s⁻¹. The testing temperature is 165 °C

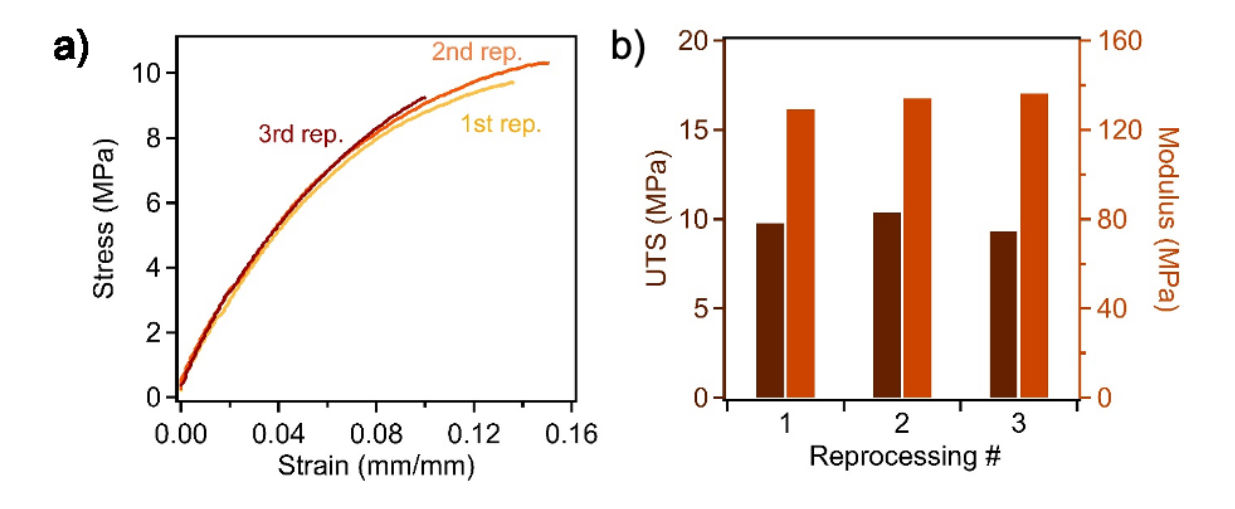


Figure S16: Mechanical properties of PP_v -1000-1.6 after reprocessing three times via melt pressing and then tensile testing, where (a) shows the stress strain curves and (b) shows the extracted ultimate tensile strength (UTS) and modulus of the materials after reprocessing.

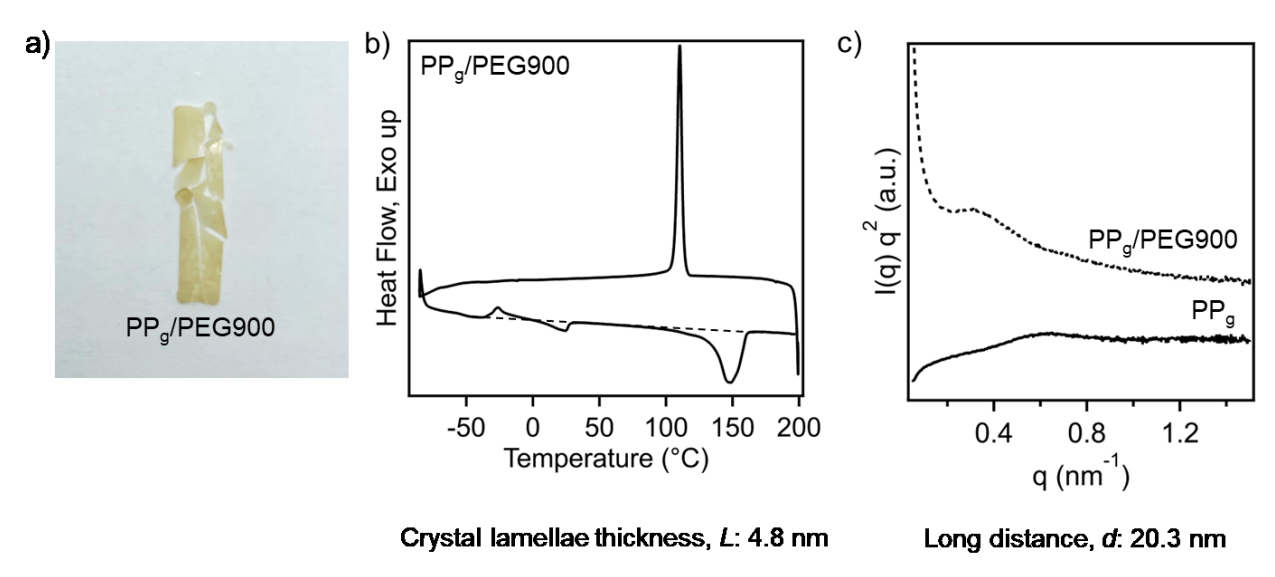


Figure S17. (a) Photo of PP_g/PEG900 blend after melt pressing, showing this blend is too fragile to remove from the mold. (b) DSC thermogram of PP_g/PEG900 blend showing the cooling (top) and second heating (bottom) curves. (c) Lorentz corrected SAXS plots of PP_g (solid) and PP_g/PEG900 blend (dashed).

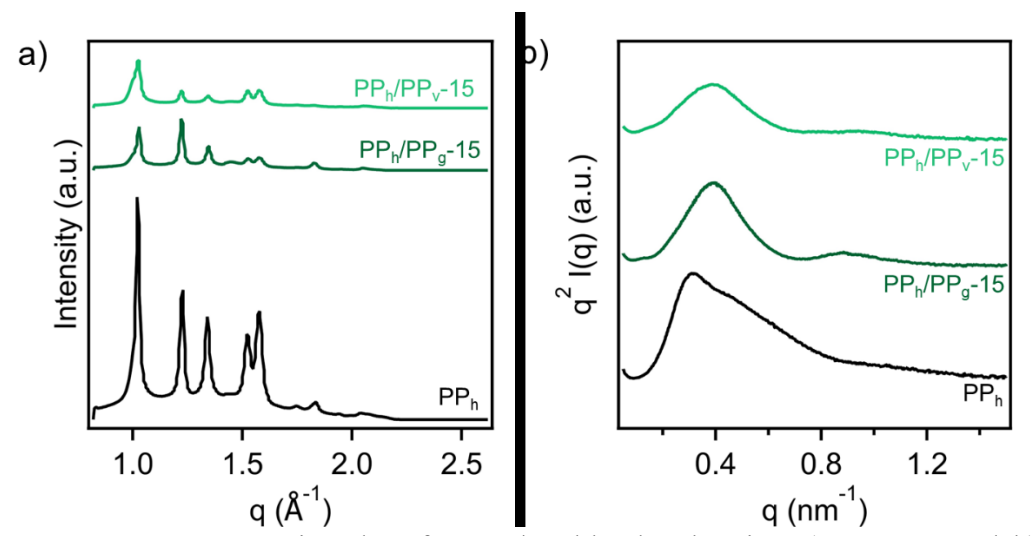


Figure S18. X-ray scattering data for PP_h/PP blends, showing a) WAXS, and b) SAXS after Lorentz-correction.

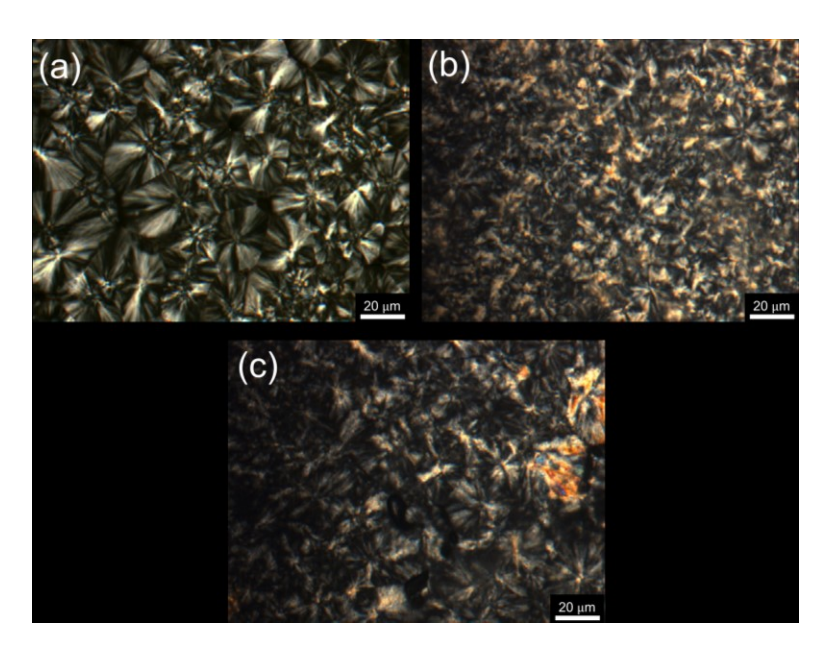


Figure S19. polarized optical microscopy measurements of (a) PP_h , (b) PP_h/PP_g blends (15 wt% PP_g), and (c) PP_h/PP_v blends (15 wt% PP_v) under isothermal crystallization at 125 °C, where no obvious phase separation were observed.

Name	Polymer source	Crosslinker type	$\frac{[PEG]}{[MA]}$	Crosslinker content (vol%)	Crosslinker content (wt%)	Reaction temp. (°C)	Reaction time (min)
PPg	PP-g-MA	-	-	-	-	-	-
PP _v -200-0.8	PP-g-MA	PEG200	0.8	4.1	5.0	150	10
PP _v -200-1.2	PP-g-MA	PEG200	1.2	6.0	7.3	160	15
PP _v -200-1.6	PP-g-MA	PEG200	1.6	7.8	9.5	160	20
PP _v -1000-0.8	PP-g-MA	PEG1000	0.8	16.9	20.7	150	15
PP _v -1000-1.2	PP-g-MA	PEG1000	1.2	23.4	28.1	160	20
PP _v -1000-1.6	PP-g-MA	PEG1000	1.6	29.0	34.3	160	20

Table S1. Sample names, composition ratios, and reaction conditions.

Sample	T_m (°C)	$X_{c,PP}$ (%)	L (nm)	d (nm)
PPg	155.5	39.2	5.5	9.5
PP _v -200-0.8	148.1	38.0	4.8	14.4
PP _v -200-1.2	148.6	37.2	4.8	12.8
PP _v -200-1.6	149.2	35.7	4.9	14.7
PP _v -1000-0.8	148.4	38.7	4.8	12.5
PP _v -1000-1.2	149.4	33.0	4.9	27.2

PP_v**-1000-1.6** 150.9 32.1 5.0 29.4

Table S2. Melting temperature and crystallinity of PP domain (via DSC) used for characterizing the structure of PP_g and PP_v through lamellar thickness and long period.

Experimental Section for determining viscosity average molecular weight of PPh

"PP samples were dissolved in decalin at 150 °C before being transferred to a D963 Ubbelohde viscosity capillary tube submerged in an oil bath set at 135 °C. Once transferred, samples were allowed to equilibrate at 135 °C before elution times were recorded. Four concentrations were prepared, ranging from 0.00025 to 0.001 g/ml. Once the elution times were recorded and the specific viscosity was determined, intrinsic viscosity was calculated based on the y-intercept value of the reduced viscosity vs. concentration plot, as based on the equation below:

$$[\eta] = \lim_{c \to 0} \frac{\eta_{sp}}{c}$$

where $[\eta]$ represents the intrinsic viscosity, η_{sp} represents specific viscosity, c represents concentration, and $\frac{\eta_{sp}}{c}$ represents reduced viscosity. The calculated intrinsic viscosity was then utilized to calculate the viscosity average molecular weight (Mv) of the polypropylene sample, employing the Mark-Houwink equation listed below:

In this equation $[\eta]$ represents intrinsic viscosity, M represents viscosity average molecular weight, and K and α are constants which are determined based on the solvent, polymer, and temperature used. For the purposes of this experiment, the K and α constants were utilized from a reference and were 0.00011 dl/g and 0.80, respectively. The Mv for the polypropylene employed was calculated to be approximately 1.6 x 10^5 g/mol."